JHEP

Published for SISSA by Springer

Received: October 19, 2022
Revised: January 16, 2023
Accepted: March 17, 2023
Published: March 27, 2023

Status of the singlino-dominated dark matter in general Next-to-Minimal Supersymmetric Standard Model

Junjie Cao,[a,b,1] **Xinglong Jia,**[a] **Lei Meng,**[a] **Yuanfang Yue**[a,1] **and Di Zhang**[a,1]

[a] *School of Physics, Henan Normal University,*
46# East of Construction Road, Xinxiang 453007, Henan, China
[b] *School of Physics, Shandong University,*
27# South of Shanda Road, Jinan 250100, Shandong, China

E-mail: junjiec@alumni.itp.ac.cn, JiaXinglong1996@outlook.com, mel18@foxmail.com, yueyuanfang@htu.edu.cn, dz481655@gmail.com

Abstract: With the rapid progress of dark matter direct detection experiments, the attractiveness of the popular bino-dominated dark matter in economical supersymmetric theories is fading. As an alternative, the singlino-dominated dark matter in general Next-to-Minimal Supersymmetric Standard Model (NMSSM) is paying due attention. This scenario has the following distinct characteristics: free from the tadpole problem and the domain-wall problem of the NMSSM with a Z_3-symmetry, predicting more stable vacuum states than the Z_3-NMSSM, capable of forming an economical secluded dark matter sector to yield the dark matter experimental results naturally, and readily weaken the restrictions from the LHC search for SUSY. Consequently, it can explain the muon g-2 anomaly in broad parameter space that agrees with various experimental results while simultaneously breaking the electroweak symmetry naturally. In this study, we show in detail how the scenario coincides with the experiments, such as the SUSY search at the LHC, the dark matter search by the LZ experiment, and the improved measurement of the muon g-2. We provide a simple and clear picture of the physics inherent in the general NMSSM.

Keywords: Extended Supersymmetry, Models for Dark Matter, Supersymmetry, Supersymmetry Breaking

ArXiv ePrint: 2210.08769

[1] Corresponding author.

https://doi.org/10.1007/JHEP03(2023)198

JHEP03(2023)198

Contents

1 Introduction **1**

2 Theoretical preliminaries of GNMSSM **5**
- 2.1 Higgs sector 5
- 2.2 Neutralino sector 7
- 2.3 Muon g-2 9
- 2.4 LHC search for SUSY 10

3 Status of singlino-dominated DM **14**
- 3.1 Research strategy 15
- 3.2 Key features of the results 16
- 3.3 Impact of the LZ experiment 21
- 3.4 Benchmark points 23
- 3.5 More discussions of the results 26

4 Summary **29**

1 Introduction

Thanks to the rapid progress of particle physics experiments in recent years, rich information about supersymmetry (SUSY) has been accumulated. The Run-II data of the Large Hadron Collider (LHC) enable scientists to explore the properties of winos and higgsinos with their masses up to about 1060 GeV for $m_{\tilde{\chi}_1^0} \lesssim 400$ GeV and 900 GeV for $m_{\tilde{\chi}_1^0} \lesssim 240$ GeV [1], respectively, where $\tilde{\chi}_1^0$ denotes the lightest neutralino acting as the lightest supersymmetric particle (LSP), and thus dark matter (DM) candidate under the assumption of R-parity conservation [2], and $m_{\tilde{\chi}_1^0}$ is its mass. The data also exclude with statistical methods squarks lighter than approximate 1850 GeV when the LSP is massless [3, 4]. Further, the combined measurement of the muon anomalous magnetic moment, $a_\mu \equiv (g-2)_\mu/2$, by the E989 experiment at Fermilab Laboratory [5] and the E821 experiment at the Brookhaven National Laboratory (BNL) [6] indicates a 4.2σ discrepancy from the Standard Model's prediction [7–27]. Although this difference may be caused by the uncertainties in calculating the hadronic contribution to the moment, as suggested by the recent lattice simulation of the BMW collaboration [28], it was widely conjectured to arise from new physics beyond the SM (see, e.g., ref. [29] and the references therein). Along this direction, it is remarkable that once the difference is confirmed to originate from SUSY effects, salient features of the theory, e.g., the mass spectra of the electroweakinos and sleptons, will be revealed [30–83]. In addition, the LUX-ZEPLIN (LZ) experiment just released its first results about the direct search for DM, where the sensitivities to spin-independent (SI) and spin-dependent

JHEP03(2023)198

(SD) cross-sections of DM-nucleon scattering have reached about $6.0 \times 10^{-48}\,\mathrm{cm}^2$ and $1.0 \times 10^{-42}\,\mathrm{cm}^2$, respectively [84], when the DM mass ranges from 20 GeV to 40 GeV. These unprecedent precisions limit strongly the DM couplings to the SM particles. Given that these remarkable achievements reflect different aspects of SUSY, we are motivated to survey their combined impacts on the theory.

As an economical realization of SUSY, Next-to-Minimal Supersymmetric Standard Model (NMSSM) predicts several viable DM candidates. On the premise of explaining both the experimentally measured density of the DM in the universe and the muon g-2 anomaly, the candidate must be bino- or singlino-dominated lightest neutralino [68, 82].[1] Concerning the former case, the cross-sections of the DM-nucleon scattering are approximated by [87, 88]

$$\sigma^{\mathrm{SI}}_{\tilde{\chi}^0_1-N} \simeq 5 \times 10^{-45}\mathrm{cm}^2 \left(\frac{C_{\tilde{\chi}^0_1\tilde{\chi}^0_1 h}}{0.1}\right)^2 \left(\frac{m_h}{125\,\mathrm{GeV}}\right)^2, \tag{1.1}$$

$$\sigma^{\mathrm{SD}}_{\tilde{\chi}^0_1-N} \simeq C_N \times \left(\frac{C_{\tilde{\chi}^0_1\tilde{\chi}^0_1 Z}}{0.1}\right)^2, \tag{1.2}$$

where $C_p \simeq 1.8 \times 10^{-40}\,\mathrm{cm}^2$ for protons, $C_n \simeq 1.4 \times 10^{-40}\,\mathrm{cm}^2$ for neutrons, and $C_{\tilde{\chi}^0_1\tilde{\chi}^0_1 h}$ and $C_{\tilde{\chi}^0_1\tilde{\chi}^0_1 Z}$ represent DM couplings to the SM-like Higgs boson discovered at the LHC and Z-boson, respectively. These couplings take the following form [89–91]

$$\begin{aligned} C_{\tilde{\chi}^0_1\tilde{\chi}^0_1 h} &\simeq e \tan\theta_W \frac{m_Z}{\mu(1 - m^2_{\tilde{\chi}^0_1}/\mu^2)} \left(\cos(\beta+\alpha) + \sin(\beta-\alpha)\frac{m_{\tilde{\chi}^0_1}}{\mu}\right) \\ &\simeq e \tan\theta_W \frac{m_Z}{\mu(1 - m^2_{\tilde{\chi}^0_1}/\mu^2)} \left(\sin 2\beta + \frac{m_{\tilde{\chi}^0_1}}{\mu}\right), \end{aligned} \tag{1.3}$$

$$C_{\tilde{\chi}^0_1\tilde{\chi}^0_1 Z} \simeq \frac{e \tan\theta_W \cos 2\beta}{2} \frac{m_Z^2}{\mu^2 - m^2_{\tilde{\chi}^0_1}}, \tag{1.4}$$

where θ_W is the weak mixing angle, $m_{\tilde{\chi}^0_1}$ denotes the lightest neutralino mass that relates with the bino mass M_1 by $m_{\tilde{\chi}^0_1} \simeq M_1$, μ represents higgsino mass, $\tan\beta = v_u/v_d$ is the ratio of Higgs vacuum expectation values, and α is the mixing angle of the CP-even Higgs states. The formulae indicate that the DM direct detection experiments alone can set a lower bound on the magnitude of μ. In ref. [82], we performed a sophisticated scan over the parameter space of the NMSSM with a discrete Z_3-symmetry (Z_3-NMSSM) to explain the muon g-2 anomaly. During this process, we considered the constraints from the DM direct search experiment XENON-1T [92, 93] and the LHC search for SUSY. We found that the XENON-1T experiment had set the limit $\mu \gtrsim 300\,\mathrm{GeV}$, and the LHC constraints could further improve it to about 450 GeV. In addition, if one replaces the XENON-1T restrictions with the LZ restrictions to reanalyze the samples obtained in the scan, the bounds become about 380 GeV and 550 GeV, respectively. We emphasized that the enhanced bounds on

[1] In the case that the lightest left-handed sneutrino acts as a DM candidate, its interaction with Z-boson predicts a much smaller density than its measured value, i.e., $\Omega\hbar^2 \ll 0.12$, and meanwhile an unacceptably large DM-nucleon scattering rate [85]. For wino- or higgsino-dominated DM case, the density is at the order of 10^{-3} by our calculation. These cases were surveyed in MSSM to explain the muon g-2 anomaly in ref. [86].

JHEP03(2023)198

μ have at least two important implications. One is that it deteriorates the naturalness in the electroweak symmetry breaking, which is reflected by the need for more fine-tuned cancellations to obtain Z-boson mass [94]. The other is that the heavy higgsinos prefer moderately light gauginos and/or sleptons to explain the muon g-2 anomaly, which can significantly strengthen the LHC restrictions. Specifically, the Bayesian evidence obtained in ref. [82] is reduced by a factor of about 6 when the LZ experiment is used to limit the Z_3-NMSSM. This result reflects an intrinsic tension between the improving DM direct search experiments and the LHC experiments in explaining the anomaly. Consequently, the bino-dominated DM case is becoming tightly limited, given the smooth advancement of the DM direct detection experiments.[2] This feature makes it less attractive.

The singlino-dominated DM differs from the bino-dominated one in that both $C_{\tilde{\chi}_1^0\tilde{\chi}_1^0 h}$ and $C_{\tilde{\chi}_1^0\tilde{\chi}_1^0 Z}$ are proportional to λ^2 when the LHC-discovered scalar has the same properties as the SM Higgs boson [87, 95, 96], where λ denotes the singlet-doublet Higgs Yukawa coupling in superpotential. Evidently, this type of DM can readily satisfy the constraints from the DM direct detection experiments when λ is small. In the Z_3-NMSSM, the DM usually obtains the measured relic density either by annihilating into $t\bar{t}$ state through an off-shell Z-boson exchange or by co-annihilating with higgsino-dominated electroweakinos [87, 95]. The former case happens for $0.4 \lesssim \lambda \lesssim 0.7$. Although its prediction on the SI cross-section may be less than $10^{-47}\mathrm{cm}^2$ due to the cancellation of different contributions shown in figure 2 of ref. [95], the SD cross-section is always at the order of $10^{-41}\mathrm{cm}^2$, which contradicts to the recent LZ experimental limits. The latter case is tenable within a narrow parameter space characterized by $2|\kappa|/\lambda \simeq 1$, $\lambda \lesssim 0.1$, and $\mu \lesssim 400\,\mathrm{GeV}$, where κ parameterizes the singlet Higgs field's self-coupling. Even without the demand to explain the muon g-2 anomaly, its Bayesian evidence is heavily suppressed, indicating that the case needs tuning of its parameters to survive experimental constraints. In addition, it should be noted that the singlino-dominated dark matter may also achieve the measured density through the resonant annihilation into singlet-dominated CP-even or -odd Higgs boson [91, 97–109]. This mechanism, however, becomes less favored by the improving DM direct detection experiments. The fundamental reason is that smaller and smaller λ and κ (note that $|\kappa| < \lambda/2$ in the Z_3-NMSSM to obtain the singlino-dominated DM), as required by the direct detection experiments, will reduce the DM's coupling strength with the scalars. As a result, $2|m_{\tilde{\chi}_1^0}|$ must be closer to the scalar mass to obtain the measured density. This situation requires the fine-tuning quantity, defined in eq. (19) of ref. [110] to get the measured density, to be larger than about 150. It will deteriorate if a smaller density is demanded to avoid the over-closure of the universe. So the mechanism contributes little to the Bayesian evidence in an elaborated scan of the model's parameter space with the MultiNest algorithm [111] and is, therefore, usually neglected. In the footnote 6 of this work, we will discuss more about this subject.

The deficit of the Z_3-NMSSM is amended in the general NMSSM (GNMSSM), where the relationship $2|\kappa|/\lambda < 1$ in the Z_3-NMSSM does not hold [96]. Specifically, the singlet-

[2]Recently, three authors of this work, namely X. Jia, L. Meng, and Y. Yue, surveyed the Minimal Supersymmetric Standard Model (MSSM) similarly to this study. They took great pains to explore the theory's parameter space in detail and confirmed the above conclusions.

JHEP03(2023)198

dominated particles, such as the singlino-dominated DM and singlet-dominated Higgs bosons, can form a secluded DM sector, where κ controls the couplings among these particles. In this case, the singlino-dominated DM achieves the measured relic density by annihilating into a pair of the singlet-dominated Higgs bosons [96]. Other distinct features of the GNMSSM include [68]

- The LHC restrictions on sparticle mass spectra are significantly relaxed since heavy sparticles tend to decay first into lighter sparticles other than the singlino-dominated DM. Consequently, the decay chain is lengthened, and the decay product becomes complicated.

- The muon g-2 anomaly can be explained by light higgsinos, favored in natural electroweak symmetry breaking. This situation is in sharp contrast with the bino-dominated DM case.

- The DM direct detection experiments prefer a small λ, which is beneficial to stabilize the vacuum of the scalar potential in the GNMSSM.

In the GNMSSM, the SM-like Higgs boson may be the lightest CP-even Higgs state or next-to-lightest CP-even Higgs state, which is dubbed as h_1-scenario and h_2-scenario, respectively, in literature. We showed in ref. [82] that the h_2-scenario is featured by $\tan\beta \lesssim 30$ and moderately light higgsinos, $\mu_{\rm tot} \lesssim 500\,{\rm GeV}$. If required to account for the muon g-2 anomaly, it entails some light sparticles which make the LHC constraints very tight. As a result, the scenario is hard to keep consistent with all experimental data. Therefore, we concentrate on the h_1-scenario in this study to survey the status of the singlino-dominated DM, given the great progress of the LHC experiments, the DM direct detection experiments, and the muon g-2 measurement in recent years. This work differs from the previous study of μ-term extended NMSSM (μNMSSM) in following aspects [68, 82]. First, the GNMSSM comprises the μNMSSM and thus provides more flexible mechanisms to be compatible with experiments. For example, the mass for the singlet-dominated Higgs bosons in the GNMSSM can be treated as free parameters. Thus, the theory opens up more DM annihilation channels than the μNMSSM to affect the relic density. Second, some additional analyses of the LHC data, such as the latest ATLAS search for tri-lepton + $E_T^{\rm miss}$ signal [112], are implemented in this study. They provide more stringent constraints on the theory. Last, the impact of the recent LZ experiment on the GNMSSM is scrutinized, which can further strengthen the experimental restrictions on the GNMSSM.

This work is organized as follows. In section 2, we briefly introduce the basics of GNMSSM and the SUSY contribution to a_μ. In section 3, we perform a sophisticated scan over the broad parameter space of the GNMSSM and investigate the status of the singlino-dominated DM in view of the experimental advancements. We also survey the impact of the recent LZ experiment on the GNMSSM. Lastly, we draw conclusions in section 4.

JHEP03(2023)198

2 Theoretical preliminaries of GNMSSM

The superpotential of the GNMSSM is given by [113–115]

$$W_{\rm GNMSSM} = W_{\rm Yukawa} + \lambda \hat{S}\hat{H}_u \cdot \hat{H}_d + \frac{\kappa}{3}\hat{S}^3 + \mu \hat{H}_u \cdot \hat{H}_d + \xi \hat{S} + \frac{1}{2}\mu' \hat{S}^2, \tag{2.1}$$

where the Yukawa terms contained in $W_{\rm Yukawa}$ are the same as those of the MSSM, $\hat{H}_u = (\hat{H}_u^+, \hat{H}_u^0)^T$ and $\hat{H}_d = (\hat{H}_d^0, \hat{H}_d^-)^T$ represent $\mathrm{SU}(2)_L$ doublet Higgs superfields, and λ, κ are dimensionless coupling coefficients parameterizing the Z_3-invariant trilinear terms. Historically, the Z_3-symmetry violating terms, characterized by the bilinear mass parameters μ, μ' and the singlet tadpole parameter ξ, were introduced to solve the tadpole problem [113, 116] and the cosmological domain-wall problem of the Z_3-NMSSM [117–119]. The bilinear terms might stem from an underlying discrete R symmetry, Z_4^R or Z_8^R, after SUSY breaking, and could be naturally at the electroweak scale [117, 120–123]. They can change significantly the properties of the Higgs bosons and the neutralinos in the Z_3-NMSSM and lead to much richer phenomenology. The ξ-term can be eliminated by shifting the $\hat{S}$ field with a constant and redefining the μ parameter [122]. So, without loss of generality, ξ is set to be zero in this study.

2.1 Higgs sector

The soft-breaking terms for the Higgs fields take the following form [113, 114]:

$$\begin{aligned} -\mathcal{L}_{\rm soft} = &\left[\lambda A_\lambda S H_u \cdot H_d + \frac{1}{3}A_\kappa \kappa S^3 + m_3^2 H_u \cdot H_d + \frac{1}{2}{m'_S}^2 S^2 + h.c.\right] \\ &+ m_{H_u}^2 |H_u|^2 + m_{H_d}^2 |H_d|^2 + m_S^2 |S|^2, \end{aligned} \tag{2.2}$$

where H_u, H_d and S represent the scalar components of the Higgs superfields, and their squared masses, $m_{H_u}^2$, $m_{H_d}^2$ and m_S^2, can be fixed by solving the conditional equations to minimize the scalar potential and expressed in terms of the vevs of the Higgs fields, which are denoted as $\langle H_u^0 \rangle = v_u/\sqrt{2}$, $\langle H_d^0 \rangle = v_d/\sqrt{2}$ and $\langle S \rangle = v_s/\sqrt{2}$ with $v = \sqrt{v_u^2 + v_d^2} \simeq 246$ GeV. As usual, an effective μ-parameter is defined by $\mu_{\rm eff} \equiv \lambda v_s/\sqrt{2}$. After these arrangements, the Higgs sector is described by ten free parameters: $\tan\beta$, the Yukawa couplings λ and κ, $\mu_{\rm eff}$, the soft-breaking trilinear coefficients A_λ and A_κ, the bilinear mass parameters μ and μ', and their soft-breaking parameters m_3^2 and ${m'_S}^2$.

In revealing the characteristics of the Higgs physics, it is customary to work with the following field combinations: $H_{\rm SM} \equiv \sin\beta {\rm Re}(H_u^0) + \cos\beta {\rm Re}(H_d^0)$, $H_{\rm NSM} \equiv \cos\beta {\rm Re}(H_u^0) - \sin\beta {\rm Re}(H_d^0)$, and $A_{\rm NSM} \equiv \cos\beta {\rm Im}(H_u^0) - \sin\beta {\rm Im}(H_d^0)$, where $H_{\rm SM}$ stands for the SM Higgs field, and $H_{\rm NSM}$ and $A_{\rm NSM}$ represent the beyond-SM doublet fields [124]. The elements of CP-even Higgs boson mass matrix $\mathcal{M}_S^2$ in the bases $(H_{\rm NSM}, H_{\rm SM}, {\rm Re}[S])$ are read as

JHEP03(2023)198

follows [113]:

$$
\begin{aligned}
\mathcal{M}^2_{S,11} &= \frac{2\left[\mu_{\rm eff}(\lambda A_\lambda + \kappa\mu_{\rm eff} + \lambda\mu') + \lambda m_3^2\right]}{\lambda \sin 2\beta} + \frac{1}{2}(2m_Z^2 - \lambda^2 v^2)\sin^2 2\beta, \\
\mathcal{M}^2_{S,12} &= -\frac{1}{4}(2m_Z^2 - \lambda^2 v^2)\sin 4\beta, \\
\mathcal{M}^2_{S,13} &= -\frac{1}{\sqrt{2}}(\lambda A_\lambda + 2\kappa\mu_{\rm eff} + \lambda\mu')v\cos 2\beta, \\
\mathcal{M}^2_{S,22} &= m_Z^2\cos^2 2\beta + \frac{1}{2}\lambda^2 v^2 \sin^2 2\beta, \\
\mathcal{M}^2_{S,23} &= \frac{v}{\sqrt{2}}\left[2\lambda(\mu_{\rm eff} + \mu) - (\lambda A_\lambda + 2\kappa\mu_{\rm eff} + \lambda\mu')\sin 2\beta\right], \\
\mathcal{M}^2_{S,33} &= \frac{\lambda(A_\lambda + \mu')\sin 2\beta}{4\mu_{\rm eff}}\lambda v^2 + \frac{\mu_{\rm eff}}{\lambda}\left(\kappa A_\kappa + \frac{4\kappa^2\mu_{\rm eff}}{\lambda} + 3\kappa\mu'\right) - \frac{\mu}{2\mu_{\rm eff}}\lambda^2 v^2,
\end{aligned}
\tag{2.3}
$$

and those for CP-odd Higgs fields in the bases $(A_{\rm NSM}, {\rm Im}(S))$ are given by equations (2.4):

$$
\begin{aligned}
\mathcal{M}^2_{P,11} &= \frac{2\left[\mu_{\rm eff}(\lambda A_\lambda + \kappa\mu_{\rm eff} + \lambda\mu') + \lambda m_3^2\right]}{\lambda \sin 2\beta}, \\
\mathcal{M}^2_{P,22} &= \frac{(\lambda A_\lambda + 4\kappa\mu_{\rm eff} + \lambda\mu')\sin 2\beta}{4\mu_{\rm eff}}\lambda v^2 - \frac{\kappa\mu_{\rm eff}}{\lambda}(3A_\kappa + \mu') - \frac{\mu}{2\mu_{\rm eff}}\lambda^2 v^2 - 2{m'_S}^2, \\
\mathcal{M}^2_{P,12} &= \frac{v}{\sqrt{2}}(\lambda A_\lambda - 2\kappa\mu_{\rm eff} - \lambda\mu').
\end{aligned}
\tag{2.4}
$$

The mass eigenstates $h_i = \{h, H, h_s\}$ and $a_i = \{A_H, A_s\}$ are obtained by unitary rotations V and V_P to diagonalize $\mathcal{M}^2_S$ and $\mathcal{M}^2_P$, respectively, leading to the following decompositions:

$$
h_i = V^{\rm NSM}_{h_i} H_{\rm NSM} + V^{\rm SM}_{h_i} H_{\rm SM} + V^{\rm S}_{h_i} Re[S], \qquad a_i = V^{\rm NSM}_{P,a_i} A_{\rm NSM} + V^{\rm S}_{P,a_i} Im[S]. \tag{2.5}
$$

Among these states, h denotes the SM-like scalar discovered at the LHC, H and A_H represent the heavy doublet-dominated states, and h_s and A_s are the singlet-dominated states. For convenience, these states are also labelled in ascending mass orders, i.e. $m_{h_1} < m_{h_2} < m_{h_3}$, and $m_{A_1} < m_{A_2}$. Thus, $h \equiv h_1$ and $m_{h_s} > m_h$ in the h_1-scenario. The mass of the charged Higgs state $H^\pm = \cos\beta H_u^\pm + \sin\beta H_d^\pm$ is given in equation (2.6):

$$
m^2_{H^\pm} = m_A^2 + m_W^2 - \lambda^2 v^2, \tag{2.6}
$$

where $m_A^2 \equiv 2\left[\mu_{\rm eff}(\lambda A_\lambda + \kappa\mu_{\rm eff} + \lambda\mu') + \lambda m_3^2\right]/(\lambda \sin 2\beta)$ represents the squared mass of the $A_{\rm NSM}$ field. So far, extra Higgs bosons, H, A_H, h_s, A_s and $H^\pm$, have been searched for intensively at the LHC (see, e.g., refs. [125, 126]), and model-independent upper limits on their production rate are acquired.

JHEP03(2023)198

In the limit of $\lambda \to 0$, $m_A^2 \simeq 2m_3^2/\sin 2\beta$, and the mass matrix elements are approximated by[3]

$$\begin{aligned}
&\mathcal{M}_{S,11}^2 \simeq m_A^2 + m_Z^2 \sin^2 2\beta, \quad && \mathcal{M}_{S,12}^2 \simeq -\frac{1}{2} m_Z^2 \sin 4\beta, && \mathcal{M}_{S,13}^2 \simeq 0, \\
&\mathcal{M}_{S,22}^2 \simeq m_Z^2 \cos^2 2\beta, && \mathcal{M}_{S,23}^2 \simeq 0, && \mathcal{M}_{S,33}^2 \simeq \frac{\mu_{\rm eff}}{\lambda}\left(\kappa A_\kappa + \frac{4\kappa^2 \mu_{\rm eff}}{\lambda} + 3\kappa\mu'\right), \\
&\mathcal{M}_{P,11}^2 = m_A^2, && \mathcal{M}_{P,22}^2 \simeq -\frac{\kappa \mu_{\rm eff}}{\lambda}(3A_\kappa + \mu') - 2{m'_S}^2, && \mathcal{M}_{P,12}^2 \simeq 0.
\end{aligned} \tag{2.7}$$

These formulae reflect the following facts [82]:

- Parameters A_λ and m_3 determine the masses of the heavy doublet-dominated scalars. Given a small λ preferred by the LZ restriction on the singlino-dominated DM scenario, they affect little the other Higgs bosons' properties.
- Parameters A_κ and m'_S appear only in $\mathcal{M}_{S,33}^2$ and $\mathcal{M}_{P,22}^2$, which implies that m_{h_s} and m_{A_s} can vary freely by adjusting A_κ and m'_S. This situation is different from that of the Z_3-NMSSM, where $\mu_{\rm tot} \equiv \mu_{\rm eff}$, $\mu' = 0$, and $m'_S = 0$, and consequently the masses of singlet fields are correlated [110]. In this study, we are particularly interested in the mass hierarchy $m_{h_s}, m_{A_s} \ll m_A$ since the singlet-dominated scalars play crucial roles in the DM annihilation.

Given that too many parameters are involved in the Higgs sector, we study the h_1-scenario by assuming the charged Higgs bosons to be massive through setting $A_\lambda = 500\,\text{GeV}$ and $m_3 = 250\,\text{GeV}$. Specifically, it is found that $m_{H^\pm}$ ranges from about 1050 GeV to about 5000 GeV in this study, which is consistent with the constraints from the LHC search for $H^\pm$ [126].

2.2 Neutralino sector

The neutralino sector of the GNMSSM comprises bino field $\tilde{B}$, wino field $\tilde{W}$, higgsino fields $\tilde{H}_d^0$ and $\tilde{H}_u^0$, and singlino field $\tilde{S}$. Its mass matrix in the bases $(-i\tilde{B}, -i\tilde{W}, \tilde{H}_d^0, \tilde{H}_u^0, \tilde{S})$ takes the following form [113], as shown in equation (2.8):

$$M_{\tilde{\chi}^0} = \begin{pmatrix}
M_1 & 0 & -m_Z \sin\theta_W \cos\beta & m_Z \sin\theta_W \sin\beta & 0 \\
 & M_2 & m_Z \cos\theta_W \cos\beta & -m_Z \cos\theta_W \sin\beta & 0 \\
 & & 0 & -\mu_{\rm tot} & -\frac{1}{\sqrt{2}}\lambda v \sin\beta \\
 & & & 0 & -\frac{1}{\sqrt{2}}\lambda v \cos\beta \\
 & & & & \frac{2\kappa}{\lambda}\mu_{\rm eff} + \mu'
\end{pmatrix}, \tag{2.8}$$

where M_1 and M_2 denote gaugino soft-breaking masses, and $\mu_{\rm tot} \equiv \mu_{\rm eff} + \mu$ represents the higgsino mass. With a rotation matrix N to diagonalize this mass matrix, neutralino mass eigenstates are expressed by equation (2.9):

$$\tilde{\chi}_i^0 = N_{i1}\psi_1^0 + N_{i2}\psi_2^0 + N_{i3}\psi_3^0 + N_{i4}\psi_4^0 + N_{i5}\psi_5^0, \tag{2.9}$$

[3] Given $\mu_{\rm eff} \equiv \lambda v_s/\sqrt{2}$ and $\mu_{\rm eff} \lesssim 30\text{GeV}$ indicated by numerical results of this study (see discussions below), we also neglect terms proportional to $\mu_{\rm eff}$ in the mass matrices. It agrees with the approximation of $2\kappa\mu_{\rm eff} \simeq \lambda m_{\tilde{\chi}_1^0} - \lambda\mu'$, indicated by the first expression in eq. (2.10).

JHEP03(2023)198

where $\tilde{\chi}_i^0$ $(i = 1, 2, 3, 4, 5)$ are labeled in an ascending mass order, N_{i3} and N_{i4} characterize the $\tilde{H}_d^0$ and $\tilde{H}_u^0$ components in $\tilde{\chi}_i^0$, respectively, and N_{i5} represents the singlino component.

Assuming $|m^2_{\tilde{\chi}_1^0} - \mu^2_{\rm tot}| \gg \lambda^2 v^2$ and very massive gauginos,[4] the mass of the singlino-dominated $\tilde{\chi}_1^0$ and its field compositions are approximated by [91, 127, 128]

$$m_{\tilde{\chi}_1^0} \simeq \frac{2\kappa}{\lambda}\mu_{\rm eff} + \mu' + \frac{1}{2}\frac{\lambda^2 v^2 (m_{\tilde{\chi}_1^0} - \mu_{\rm tot}\sin 2\beta)}{m^2_{\tilde{\chi}_1^0} - \mu^2_{\rm tot}}, \quad N_{11} \sim 0, \quad N_{12} \sim 0, \tag{2.10}$$

$$\frac{N_{13}}{N_{15}} = \frac{\lambda v}{\sqrt{2}\mu_{\rm tot}}\frac{(m_{\tilde{\chi}_1^0}/\mu_{\rm tot})\sin\beta - \cos\beta}{1 - \left(m_{\tilde{\chi}_1^0}/\mu_{\rm tot}\right)^2}, \qquad \frac{N_{14}}{N_{15}} = \frac{\lambda v}{\sqrt{2}\mu_{\rm tot}}\frac{(m_{\tilde{\chi}_1^0}/\mu_{\rm tot})\cos\beta - \sin\beta}{1 - \left(m_{\tilde{\chi}_1^0}/\mu_{\rm tot}\right)^2},$$

$$N_{15}^2 \simeq \left(1 + \frac{N_{13}^2}{N_{15}^2} + \frac{N_{14}^2}{N_{15}^2}\right)^{-1}$$

$$= \frac{\left[1 - (m_{\tilde{\chi}_1^0}/\mu_{\rm tot})^2\right]^2}{\left[(m_{\tilde{\chi}_1^0}/\mu_{\rm tot})^2 - 2(m_{\tilde{\chi}_1^0}/\mu_{\rm tot})\sin 2\beta + 1\right]\left(\frac{\lambda v}{\sqrt{2}\mu_{\rm tot}}\right)^2 + \left[1 - (m_{\tilde{\chi}_1^0}/\mu_{\rm tot})^2\right]^2}.$$

These analytic expressions show the following properties of the DM:

- $m_{\tilde{\chi}_1^0}$ is determined by parameters λ, κ, $\tan\beta$, $\mu_{\rm eff}$, $\mu_{\rm tot}$, and μ'. Even when λ, κ, $\tan\beta$, $\mu_{\rm eff}$, and $\mu_{\rm tot}$ are fixed, it can still vary freely by adjusting μ'. In addition, λ and κ in the GNMSSM are independent parameters in predicting $|m_{\tilde{\chi}_1^0}| < |\mu_{\rm tot}|$. These situations are different from those of the Z_3-NMSSM, where $\mu' \equiv 0$ and $\mu_{\rm tot} \equiv \mu_{\rm eff}$, and consequently $|\kappa|$ must be less than $\lambda/2$ to predict the singlino-dominated neutralino as the LSP [113].

- The field compositions in $\tilde{\chi}_1^0$ depend only on $\tan\beta$, λ, $\mu_{\rm tot}$, and $m_{\tilde{\chi}_1^0}$. Therefore, it is convenient to take the four parameters and κ as theoretical inputs in studying the $\tilde{\chi}_1^0$'s properties, where κ determines the interactions among the singlet-dominated particles. This feature contrasts with that of the Z_3-NMSSM, which needs only four input parameters, namely $\tan\beta$, λ, $\mu_{\rm tot}$, and any of $m_{\tilde{\chi}_1^0}$ or κ, to describe the properties of $\tilde{\chi}_1^0$ [95].

- The singlet-dominated particles may form a secluded DM sector [129], where the DM achieves the measured density by the process $\tilde{\chi}_1^0\tilde{\chi}_1^0 \to h_s A_s, h_s h_s, A_s A_s$ or the h_s/A_s-mediated resonant annihilation into SM particles. The former annihilation proceeds mainly through the t-channel exchange of $\tilde{\chi}_1^0$ and/or the s-channel exchange of h_s/A_s, and thus, its cross-section is controlled by the parameters κ and A_κ. The rate of the latter annihilation, however, also strongly depends on the splitting between $2|m_{\tilde{\chi}_1^0}|$ and m_{h_s/A_s}. Since this sector communicates with the SM sector only through the weak singlet-doublet Higgs mixing, the DM-nucleon scattering is naturally suppressed when λ is small.

Owing to these salient features, the GNMSSM predicts a broad parameter space consistent with current DM experimental results.

[4] Note that these assumptions are unnecessary in the $\lambda \to 0$ limit encountered in this work, where the singlino field decouples from the rest fields in the neutralino sector, and $m_{\tilde{\chi}_1^0} \simeq \sqrt{2}\kappa v_s + \mu'$.

JHEP03(2023)198

2.3 Muon g-2

The SUSY source of the muon g-2, $a_\mu^{\rm SUSY}$, mainly includes loops mediated by a smuon and a neutralino and those containing a muon-type sneutrino and a chargino [30–33]. The full one-loop contributions to $a_\mu^{\rm SUSY}$ in the NMSSM were obtained in ref. [31] and are not presented here for brevity. As an alternative, we provide the expression of $a_\mu^{\rm SUSY}$ in the mass insertion approximation [32] to reveal its key features. Specifically, at the lowest order of the approximation, the contributions to $a_\mu^{\rm SUSY}$ are divided into four types: "WHL", "BHL", "BHR", and "BLR", where W, B, H, L, and R represent wino, bino, higgsino, and left-handed and right-handed smuon fields, respectively. They arise from the Feynman diagrams involving $\tilde{W}-\tilde{H}_d$, $\tilde{B}-\tilde{H}_d^0$, $\tilde{B}-\tilde{H}_d^0$, and $\tilde{\mu}_L-\tilde{\mu}_R$ transitions, respectively, and take the following form [32, 34, 35]:

$$a_{\mu,\rm WHL}^{\rm SUSY}=\frac{\alpha_2}{8\pi}\frac{m_\mu^2 M_2\mu_{\rm tot}\tan\beta}{m_{\tilde{\nu}_\mu}^4}\left\{2f_C\left(\frac{M_2^2}{m_{\tilde{\nu}_\mu}^2},\frac{\mu_{\rm tot}^2}{m_{\tilde{\nu}_\mu}^2}\right)-\frac{m_{\tilde{\nu}_\mu}^4}{\tilde{m}_{\tilde{\mu}_L}^4}f_N\left(\frac{M_2^2}{\tilde{m}_{\tilde{\mu}_L}^2},\frac{\mu_{\rm tot}^2}{\tilde{m}_{\tilde{\mu}_L}^2}\right)\right\}, \tag{2.11}$$

$$a_{\mu,\rm BHL}^{\rm SUSY}=\frac{\alpha_Y}{8\pi}\frac{m_\mu^2 M_1\mu_{\rm tot}\tan\beta}{\tilde{m}_{\tilde{\mu}_L}^4}f_N\left(\frac{M_1^2}{\tilde{m}_{\tilde{\mu}_L}^2},\frac{\mu_{\rm tot}^2}{\tilde{m}_{\tilde{\mu}_L}^2}\right), \tag{2.12}$$

$$a_{\mu,\rm BHR}^{\rm SUSY}=-\frac{\alpha_Y}{4\pi}\frac{m_\mu^2 M_1\mu_{\rm tot}\tan\beta}{\tilde{m}_{\tilde{\mu}_R}^4}f_N\left(\frac{M_1^2}{\tilde{m}_{\tilde{\mu}_R}^2},\frac{\mu_{\rm tot}^2}{\tilde{m}_{\tilde{\mu}_R}^2}\right), \tag{2.13}$$

$$a_{\mu\rm BLR}^{\rm SUSY}=\frac{\alpha_Y}{4\pi}\frac{m_\mu^2 M_1\mu_{\rm tot}\tan\beta}{M_1^4}f_N\left(\frac{\tilde{m}_{\tilde{\mu}_L}^2}{M_1^2},\frac{\tilde{m}_{\tilde{\mu}_R}^2}{M_1^2}\right), \tag{2.14}$$

where $\tilde{m}_{\tilde{\mu}_L}$ and $\tilde{m}_{\tilde{\mu}_R}$ are soft-breaking masses for left-handed and right-handed smuon fields, respectively. The loop functions are given by

$$f_C(x,y)=\frac{5-3(x+y)+xy}{(x-1)^2(y-1)^2}-\frac{2\ln x}{(x-y)(x-1)^3}+\frac{2\ln y}{(x-y)(y-1)^3}, \tag{2.15}$$

$$f_N(x,y)=\frac{-3+x+y+xy}{(x-1)^2(y-1)^2}+\frac{2x\ln x}{(x-y)(x-1)^3}-\frac{2y\ln y}{(x-y)(y-1)^3}, \tag{2.16}$$

and they satisfy $f_C(1,1)=1/2$ and $f_N(1,1)=1/6$.

These approximations reveal the following facts:

- If all SUSY parameters involved in $a_\mu^{\rm SUSY}$ take a common value $M_{\rm SUSY}$, $a_\mu^{\rm SUSY}$ is proportional to $m_\mu^2\tan\beta/M_{\rm SUSY}^2$, indicating that the muon g-2 anomaly prefers a large $\tan\beta$ and a moderately low SUSY scale.

- It was verified that the "WHL" contribution is usually much larger than the other contributions if $\tilde{\mu}_L$ is not significantly heavier than $\tilde{\mu}_R$ [68].

- In principle, the singlino field $\tilde{S}$ enters the insertions. However, since both the $\tilde{W}-\tilde{S}$ and $\tilde{B}^0-\tilde{S}$ transitions and the $\bar{\mu}\tilde{S}\tilde{\mu}_{L,R}$ couplings vanish [113], it only appears in the "WHL", "BHL" and "BHR" loops by two more insertions at the lowest order, which correspond to the $\tilde{H}_d^0-\tilde{S}$ and $\tilde{S}-\tilde{H}_d^0$ transitions in the neutralino mass matrix in eq. (2.8). Since the DM physics prefers a small λ and the LHC search for SUSY places a lower bound of about 140 GeV for the singlino mass (see the results in figure 3 and

JHEP03(2023)198

footnote 6 of this research, which specifies the phrase "lower bound" in the Bayesian sense), the singlino-induced contributions are never significant [68]. Specifically, we survey the properties of lots of parameter points acquired in this study. For each point, we compare different $a_\mu^{\rm SUSY}$, obtained by its exact formula, by that but fixing λ at a small value of 0.005, and by the mass insertion method that entirely neglects the dependence of $a_\mu^{\rm SUSY}$ on λ, respectively. We find that the differences between these predictions are within 5% for all the considered points.

- Although the GNMSSM prediction of $a_\mu^{\rm SUSY}$ is roughly the same as that of the MSSM, except that the μ parameter in the MSSM is replaced by $\mu_{\rm tot}$, the two models predict different DM physics and sparticle signals at the LHC. Consequently, they are subject to different theoretical and experimental constraints.

In this study, we do not consider two-loop (2L) contributions to a_μ, which include 2L corrections to SM one-loop diagrams and those to SUSY one-loop diagrams [36]. Before the advent of the LHC, these contributions were estimated to be significant in the parameter space characterized by moderately light H/A_H and sparticles [36]. We utilize code GM2Calc [34] to study them by selecting several MSSM benchmark points from a related study (see footnote 2 of this work).[5] These points predict different mass orders for the W, B, H, L, and R fields, but all correspond to $\tan\beta > 50$ and $a_\mu^{1L} \simeq 2.5\times10^{-9}$, with a_μ^{1L} denoting the one-loop result of $a_\mu^{\rm SUSY}$. We find $a_\mu^{\rm 2L,photonic} \simeq -2.0\times10^{-10}$, $a_\mu^{\rm 2L,f\tilde{f}} \simeq (6.0\sim9.0)\times10^{-11}$, and $a_\mu^{\rm 2L(a)} \sim 10^{-12}$, where $a_\mu^{\rm 2L,photonic}$, $a_\mu^{\rm 2L,f\tilde{f}}$, and $a_\mu^{\rm 2L(a)}$ denote photonic 2L corrections, fermion/sfermion corrections, and corrections from the photonic Barr-Zee diagrams involving pure SUSY loops of charginos, neutralinos, and sfermions, respectively [34]. The total 2L effect is about -5% of a_μ^{1L}. In addition, we note that the code GM2Calc does not include contributions from the Barr-Zee diagrams containing top/bottom quark loops, which were denoted by $a_\mu^{\rm SUSY,ferm,2L}$ in ref. [36]. We calculate these contributions by the formulae in ref. [130]. We conclude that for $\tan\beta = 60$ and $m_A = 1\,\text{TeV}$, the corrections are -1.40×10^{-11} for the $f\gamma H$ diagrams and 1.68×10^{-11} for the $f\gamma A_H$ diagrams. These results reflect that the 2L contributions missed in this study affect little our conclusions.

2.4 LHC search for SUSY

Since some of the electroweakinos and sleptons involved in $a_\mu^{\rm SUSY}$ must be moderately light to account for the anomaly [79], they are copiously produced at the LHC and thus subjected to strong constraints from the SUSY searches at the LHC with $\sqrt{s} = 13\,\text{TeV}$. These searches usually concentrate on the theories with the R-parity conservation [148, 149], where the LSP is undetected leading to missing energy in the final states. Given the complexity of the production processes and decay modes, we scrutinize numerous signal topologies in implementing the restrictions. In tables 1 and 2, we list the experimental analyses considered in this study. We find that the following reports are particularly critical:

[5] Given that the code GM2Calc works only in the framework of MSSM [34] and that GNMSSM predicts approximately the same $a_\mu^{\rm SUSY}$ as MSSM, results of the GM2Calc about the 2L corrections can be applied to GNMSSM.

JHEP03(2023)198

Scenario	Final State	Name
$\tilde{\chi}_2^0\tilde{\chi}_1^\pm \to WZ\tilde{\chi}_1^0\tilde{\chi}_1^0$	$n\ell(n \geq 2) + nj(n \geq 0) + \mathrm{E}_\mathrm{T}^\mathrm{miss}$	CMS-SUS-20-001(137fb^{-1}) [131] ATLAS-2106-01676(139fb^{-1}) [112] CMS-SUS-17-004(35.9fb^{-1}) [132] CMS-SUS-16-039(35.9fb^{-1}) [133] ATLAS-1803-02762(36.1fb^{-1}) [134] ATLAS-1806-02293(36.1fb^{-1}) [135]
$\tilde{\chi}_2^0\tilde{\chi}_1^\pm \to \ell\tilde{\nu}\ell\tilde{\ell}$	$n\ell(n = 3) + \mathrm{E}_\mathrm{T}^\mathrm{miss}$	CMS-SUS-16-039(35.9fb^{-1}) [133] ATLAS-1803-02762(36.1fb^{-1}) [134]
$\tilde{\chi}_2^0\tilde{\chi}_1^\pm \to \tilde{\tau}\nu\ell\tilde{\ell}$	$2\ell + 1\tau + \mathrm{E}_\mathrm{T}^\mathrm{miss}$	CMS-SUS-16-039(35.9fb^{-1}) [133]
$\tilde{\chi}_2^0\tilde{\chi}_1^\pm \to \tilde{\tau}\nu\tilde{\tau}\tau$	$3\tau + \mathrm{E}_\mathrm{T}^\mathrm{miss}$	CMS-SUS-16-039(35.9fb^{-1}) [133]
$\tilde{\chi}_2^0\tilde{\chi}_1^\pm \to Wh\tilde{\chi}_1^0\tilde{\chi}_1^0$	$n\ell(n \geq 1) + nb(n \geq 0) + nj(n \geq 0) + \mathrm{E}_\mathrm{T}^\mathrm{miss}$	ATLAS-1909-09226(139fb^{-1}) [136] CMS-SUS-17-004(35.9fb^{-1}) [132] CMS-SUS-16-039(35.9fb^{-1}) [133] ATLAS-1812-09432(36.1fb^{-1})[137] CMS-SUS-16-034(35.9fb^{-1})[138] CMS-SUS-16-045(35.9fb^{-1}) [139]
$\tilde{\chi}_1^\mp\tilde{\chi}_1^\pm \to WW\tilde{\chi}_1^0\tilde{\chi}_1^0$	$2\ell + \mathrm{E}_\mathrm{T}^\mathrm{miss}$	ATLAS-1908-08215(139fb^{-1}) [140] CMS-SUS-17-010(35.9fb^{-1}) [141]
$\tilde{\chi}_1^\mp\tilde{\chi}_1^\pm \to 2\tilde{\ell}\nu(\tilde{\nu}\ell)$	$2\ell + \mathrm{E}_\mathrm{T}^\mathrm{miss}$	ATLAS-1908-08215(139fb^{-1}) [140] CMS-SUS-17-010(35.9fb^{-1}) [141]
$\tilde{\chi}_2^0\tilde{\chi}_1^\mp \to h/ZW\tilde{\chi}_1^0\tilde{\chi}_1^0, \tilde{\chi}_1^0 \to \gamma/Z\tilde{G}$ $\tilde{\chi}_1^\pm\tilde{\chi}_1^\mp \to WW\tilde{\chi}_1^0\tilde{\chi}_1^0, \tilde{\chi}_1^0 \to \gamma/Z\tilde{G}$	$2\gamma + n\ell(n \geq 0) + nb(n \geq 0) + nj(n \geq 0) + \mathrm{E}_\mathrm{T}^\mathrm{miss}$	ATLAS-1802-03158(36.1fb^{-1}) [142]
$\tilde{\chi}_2^0\tilde{\chi}_1^\pm \to ZW\tilde{\chi}_1^0\tilde{\chi}_1^0, \tilde{\chi}_1^0 \to h/Z\tilde{G}$ $\tilde{\chi}_1^\pm\tilde{\chi}_1^\mp \to WW\tilde{\chi}_1^0\tilde{\chi}_1^0, \tilde{\chi}_1^0 \to h/Z\tilde{G}$ $\tilde{\chi}_2^0\tilde{\chi}_1^0 \to Z\tilde{\chi}_1^0\tilde{\chi}_1^0, \tilde{\chi}_1^0 \to h/Z\tilde{G}$ $\tilde{\chi}_1^\mp\tilde{\chi}_1^0 \to W\tilde{\chi}_1^0\tilde{\chi}_1^0, \tilde{\chi}_1^0 \to h/Z\tilde{G}$	$n\ell(n \geq 4) + \mathrm{E}_\mathrm{T}^\mathrm{miss}$	ATLAS-2103-11684(139fb^{-1}) [143]
$\tilde{\chi}_i^{0,\pm}\tilde{\chi}_j^{0,\mp} \to \tilde{\chi}_1^0\tilde{\chi}_1^0 + \chi_\mathrm{soft} \to ZZ/H\tilde{G}\tilde{G}$	$n\ell(n \geq 2) + nb(n \geq 0) + nj(n \geq 0) + \mathrm{E}_\mathrm{T}^\mathrm{miss}$	CMS-SUS-16-039(35.9fb^{-1}) [133] CMS-SUS-17-004(35.9fb^{-1}) [132] CMS-SUS-20-001(137fb^{-1}) [131]
$\tilde{\chi}_i^{0,\pm}\tilde{\chi}_j^{0,\mp} \to \tilde{\chi}_1^0\tilde{\chi}_1^0 + \chi_\mathrm{soft} \to HH\tilde{G}\tilde{G}$	$n\ell(n \geq 2) + nb(n \geq 0) + nj(n \geq 0) + \mathrm{E}_\mathrm{T}^\mathrm{miss}$	CMS-SUS-16-039(35.9fb^{-1}) [133] CMS-SUS-17-004(35.9fb^{-1}) [132]
$\tilde{\chi}_2^0\tilde{\chi}_1^\pm \to W^*Z^*\tilde{\chi}_1^0\tilde{\chi}_1^0$	$3\ell + \mathrm{E}_\mathrm{T}^\mathrm{miss}$	ATLAS-2106-01676(139fb^{-1}) [112]
$\tilde{\chi}_2^0\tilde{\chi}_1^\pm \to Z^*W^*\tilde{\chi}_1^0\tilde{\chi}_1^0$	$2\ell + nj(n \geq 0) + \mathrm{E}_\mathrm{T}^\mathrm{miss}$	ATLAS-1911-12606(139fb^{-1}) [144] ATLAS-1712-08119(36.1fb^{-1}) [145] CMS-SUS-16-048(35.9fb^{-1}) [146]
$\tilde{\chi}_2^0\tilde{\chi}_1^\pm + \tilde{\chi}_1^\pm\tilde{\chi}_1^\mp + \tilde{\chi}_1^\pm\tilde{\chi}_1^0$	$2\ell + nj(n \geq 0) + \mathrm{E}_\mathrm{T}^\mathrm{miss}$	ATLAS-1911-12606(139fb^{-1}) [144] ATLAS-1712-08119(36.1fb^{-1}) [145] CMS-SUS-16-048(35.9fb^{-1}) [146]

Table 1. Experimental analyses of the electroweakino production processes considered in this study, which are categorized by the topologies of the SUSY signals.

JHEP03(2023)198

Scenario	Final State	Name
$\tilde{\ell}\tilde{\ell} \to \ell\ell\tilde{\chi}_1^0\tilde{\chi}_1^0$	$2\ell + \mathrm{E}_\mathrm{T}^\mathrm{miss}$	ATLAS-1911-12606(139fb^{-1}) [144]
		ATLAS-1712-08119(36.1fb^{-1}) [145]
		ATLAS-1908-08215(139fb^{-1}) [140]
		CMS-SUS-20-001(137fb^{-1}) [131]
		ATLAS-1803-02762(36.1fb^{-1}) [134]
		CMS-SUS-17-009(35.9fb^{-1}) [147]

Table 2. Same as table 1, but for the slepton production processes.

- CMS-SUS-16-039 and CMS-SUS-17-004 [132, 133]: search for electroweakino productions with two, three, or four leptons and missing transverse momentum ($\mathrm{E}_\mathrm{T}^\mathrm{miss}$) in the final states. One remarkable strategy of this analysis is that it includes all the possible final states and defines several categories by the number of leptons in the event, their flavors, and their charges to enhance the discovery potential. In the context of simplified models, the observed limit on wino-dominated $m_{\tilde{\chi}_1^\pm}$ in the chargino-neutralino production is about 650 GeV for the WZ topology, 480 GeV for the WH topology, and 535 GeV for the mixed topology.

- ATLAS-2106-01676 [112]: search for wino- or higgsino-dominated chargino-neutralino pair productions. This analysis investigates on-shell WZ, off-shell WZ, and Wh categories in the decay chain and focuses on the final state containing exactly three leptons, possible ISR jets, and $\mathrm{E}_\mathrm{T}^\mathrm{miss}$. For the wino scenario in the simplified model, the exclusion bound of $m_{\tilde{\chi}_2^0}$ is about 640 GeV for a massless $\tilde{\chi}_1^0$, and it is weakened as the mass difference between $\tilde{\chi}_2^0$ and $\tilde{\chi}_1^0$ diminishes. Specifically, $\tilde{\chi}_2^0$ should be heavier than about 500 GeV for $m_{\tilde{\chi}_1^0} = 300$ GeV (the on-shell W/Z case), 300 GeV for a positive $m_{\tilde{\chi}_1^0}$ and 35 GeV $\lesssim m_{\tilde{\chi}_2^0} - m_{\tilde{\chi}_1^0} \lesssim 90$ GeV (the off-shell W/Z case), and 220 GeV when $m_{\tilde{\chi}_2^0} - m_{\tilde{\chi}_1^0} = 15$ GeV (the extreme off-shell W/Z case). By contrast, $\tilde{\chi}_2^0$ is excluded only up to 210 GeV in mass for the off-shell W/Z case of the higgsino scenario, which occurs when $m_{\tilde{\chi}_2^0} - m_{\tilde{\chi}_1^0} = 10$ GeV or $m_{\tilde{\chi}_2^0} - m_{\tilde{\chi}_1^0} \gtrsim 35$ GeV.

- ATLAS-1911-12606 [144]: concentrate on compressed mass spectra case and search for electroweakino pair or slepton pair production, with two leptons and missing transverse momentum as the final state. The results are projected onto $\Delta m - \tilde{\chi}_2^0$ plane where $\Delta m \equiv m_{\tilde{\chi}_2^0} - m_{\tilde{\chi}_1^0}$ for the electroweakino production. It is found that the tightest bound on higgsino-dominated $\tilde{\chi}_2^0$ is 193 GeV in mass for $\Delta m \simeq 9.3$ GeV, and the optimum bound on wino-dominated $\tilde{\chi}_2^0$ is 240 GeV in mass when $\Delta m \simeq 7$ GeV. Similarly, it is found that light-flavor sleptons should be heavier than about 250 GeV for $\Delta m_{\tilde{\ell}} = 10$ GeV, where $m_{\tilde{\ell}} \equiv m_{\tilde{\ell}} - m_{\tilde{\chi}_1^0}$.

- CMS-SUS-20-001 [131]: search for SUSY signal containing two oppositely charged same-flavor leptons and missing transverse momentum. This analysis studies not only strong sparticle productions, but also the electroweakino productions. The lepton originates

JHEP03(2023)198

from an on-shell or off-shell Z boson in the decay chain, or from the decay of the produced sleptons. For the electroweakino pair production, the wino-dominated chargino and neutralino are explored up to 750 GeV and 800 GeV, respectively, in mass. For the slepton pair production, the first two-generation sleptons are explored up to 700 GeV in mass.

It should be noted that although the first reports are based on the analyses of 36 fb^{-1} data, their exclusion capabilities are comparable with those of the second and fourth ones, which study the same signals but utilize 139 fb^{-1} data. It should also be noted that the search for charginos and neutralinos using fully hadronic final states of W/Z and Higgs bosons with 139 fb^{-1} data [1] is not considered. As shown in figure 12(c) of ref. [1], this analysis excludes a wino mass up to 1060 GeV when $m_{\tilde{\chi}_1^0}$ is below 400 GeV, and the mass splitting between the winos and $\tilde{\chi}_1^0$ is larger than about 400 GeV. It seems much stronger than the second report in limiting SUSY parameter space. This conclusion, however, can only be applied indirectly to this study due to the following facts. First, the results in the figure 12(c) are based on the assumption $Br(\tilde{\chi}_2^0 \to \tilde{\chi}_1^0 Z) = Br(\tilde{\chi}_2^0 \to \tilde{\chi}_1^0 h) = 50\%$ and the signals from the processes $pp \to \tilde{\chi}_2^0\tilde{\chi}_1^\pm, \tilde{\chi}_1^\pm\tilde{\chi}_1^\mp \to 2\tilde{\chi}_1^0 + WW/WZ/Wh$ in the wino scenario. The most significant contribution to $R \equiv max\{S_i/S_{i,obs}^{95}\}$, where S_i denotes the simulated event number of the i-th signal region (SR) in the analysis, and $S_{i,obs}^{95}$ represents its corresponding 95% confidence level upper limit, comes from the process $pp \to \tilde{\chi}_2^0\tilde{\chi}_1^\pm \to 2\tilde{\chi}_1^0 + Wh$. It can exclude $m_{\tilde{\chi}_2^0/\tilde{\chi}_1^\pm}$ up to 1060 GeV for massless $\tilde{\chi}_1^0$ and up to 950 GeV for $m_{\tilde{\chi}_1^0} = 400$ GeV if $Br(\tilde{\chi}_2^0 \to \tilde{\chi}_1^0 h) = 100\%$ is assumed. In contrast, the minimum contribution arises from the signal $pp \to \tilde{\chi}_1^\pm\tilde{\chi}_1^\mp \to 2\tilde{\chi}_1^0 + W^\pm W^\mp$, which can only exclude a small region on $m_{\tilde{\chi}_1^\pm} - m_{\tilde{\chi}_1^0}$ plane, characterized by $m_{\tilde{\chi}_1^0} \lesssim 90$ GeV and 640 GeV $\lesssim m_{\tilde{\chi}_1^\pm} \lesssim$ 750 GeV, for $Br(\tilde{\chi}_1^\pm \to \tilde{\chi}_1^0 W^\pm) = 100\%$. These conclusions can be inferred from figure 15 of the report. Evidently, smaller $Br(\tilde{\chi}_2^0 \to \tilde{\chi}_1^0 h)$ and $Br(\tilde{\chi}_2^0 \to \tilde{\chi}_1^0 Z)$ will weaken significantly the exclusion capability in the figure 12(c). Second, the analyses of the process $pp \to \tilde{\chi}_2^0\tilde{\chi}_1^\pm \to 2\tilde{\chi}_1^0 + WZ$ using the leptonic signal [112] and the hadronic signal [1], respectively, are compared in figure 15(b) of ref. [1]. We extract R values from this figure for some parameter points in table 3. This table indicates that the hadronic analysis is more restrictive than the leptonic analysis only when $m_{\tilde{\chi}_2^0/\tilde{\chi}_1^\pm} \gtrsim 600$ GeV for the same $m_{\tilde{\chi}_1^0}$ with $m_{\tilde{\chi}_1^0} \lesssim 300$ GeV in the wino simplified model. Similar conclusion can be acquired for the Wh signal by analyzing the process $pp \to \tilde{\chi}_2^0\tilde{\chi}_1^\pm \to 2\tilde{\chi}_1^0 + Wh$ with the leptonic and hadronic signals [1, 136], respectively, which is shown in figure 15(c) of ref. [1]. This remarkable characteristic comes from the fact that the hadronic analysis rejects large backgrounds by identifying high-p_T bosons using large-radius jets and jet substructure information, and this strategy is inefficient for low-p_T bosons. Finally, we emphasize that one of the main aims of this study is to explain the muon g-2 anomaly. Owing to the sparticle mass spectra preferred by the anomaly, the branching ratios of the wino-like particles decaying into W, Z and Higgs bosons can be suppressed significantly, and more importantly, the p_Ts of the bosons are generally softened when compared with the simplified model predictions in ref. [1]. As a result, the hadronic analysis is scarcely crucial in this study. We will return to this issue in section 3.5.

JHEP03(2023)198

	Analysis in ref. [112]			Analysis in ref. [1]		
R $m_{\tilde{\chi}_2^0/\tilde{\chi}_1^\pm}$ (GeV) / $m_{\tilde{\chi}_1^0}$ (GeV)	500	600	800	500	600	800
150	1.70	1.07	0.39	0.19	1.14	1.45
200	1.54	0.98	0.38	0.11	0.85	1.52
250	1.28	1.01	0.34	0.10	0.57	1.19
300	0.96	0.88	0.31	0.11	0.37	1.04

Table 3. Values of $R \equiv max\{S_i/S^{95}_{i,obs}\}$ for the analyses of the process $pp \to \tilde{\chi}_2^0\tilde{\chi}_1^\pm \to 2\tilde{\chi}_1^0 + WZ$ using the leptonic and hadronic signals of the vector bosons [1, 112], respectively. SUSY benchmark points in wino simplified model are considered [1]. $R > 1$ means that the point is experimentally excluded if the uncertainties involved in the calculation are neglected [68], while $R < 1$ implies that the point is consistent with the experimental analysis. Both analyses have exclusion capabilities on SUSY parameter space only when $m_{\tilde{\chi}_1^0} \lesssim 300\,\text{GeV}$, which is exhibited in figure 15(b) of ref. [1].

In summary, the GNMSSM has the following characteristics:

- $\tan\beta$, M_1, M_2, μ_{tot}, $\tilde{m}_{\tilde{\mu}_L}$, and $\tilde{m}_{\tilde{\mu}_R}$: they determine the magnitude of a_μ^{SUSY}. In particular, $\tan\beta$, M_2, μ_{tot}, and $\tilde{m}_{\tilde{\mu}_L}$ play a crucial role in explaining the muon g-2 anomaly, and the dimensional parameters have been restricted significantly by the LHC search for SUSY.

- A_λ and m_3: they determine the mass of the heavy doublet-dominated scalars, but hardly affect the other Higgs bosons' property if λ is small.

- μ_{eff}, A_κ, μ', and m'_S: they are parameters describing the properties of the singlet field S and thus are scarcely restricted by the LHC experiments. Since $m_{\tilde{\chi}_1^0}$, $m^2_{h_s}$, and $m^2_{A_s}$ depend on parameters μ', A_κ, and m'^2_S linearly in the small λ limit, these physical masses are not correlated and may vary freely within certain ranges.

- λ and κ: they are Yukawa couplings in the Higgs sector. Once the singlino-dominated $\tilde{\chi}_1^0$, h_s, and A_s form a secluded DM sector, they determine the magnitudes of the DM-nucleon scattering and the relic density, respectively.

- $m_{\tilde{t}_L}$, $m_{\tilde{t}_R}$, and A_t: they affect the mass of the SM-like Higgs boson significantly by radiative corrections.

3 Status of singlino-dominated DM

This study utilizes the package `SARAH-4.14.3` [150–153] to build the model file of the GNMSSM, the codes `SPheno-4.0.4` [154, 155] and `FlavorKit` [156] to generate particle mass spectra and compute low energy observables, such as a_μ^{SUSY} and B-physics observables, and the package `MicrOMEGAs-5.0.4` [97, 157–161] to calculate DM observables, assuming that the lightest neutralino is the sole DM candidate in the universe. Bounds from the

JHEP03(2023)198

Parameter	Prior	Range	Parameter	Prior	Range
λ	Flat	$0 \sim 0.7$	κ	Flat	$-0.7 \sim 0.7$
$\tan\beta$	Flat	$1 \sim 60$	A_κ/TeV	Flat	$-1.0 \sim 1.0$
$\mu_{\rm tot}$/TeV	Log	$0.1 \sim 1.0$	$\mu_{\rm eff}$/TeV	Log	$10^{-3} \sim 1.0$
μ'/TeV	Flat	$-1.0 \sim 1.0$	A_t/TeV	Flat	$-5.0 \sim 5.0$
M_1/TeV	Flat	$-1.5 \sim 1.5$	M_2/TeV	Log	$0.1 \sim 1.5$
$\tilde{m}_{\tilde{\mu}_L}$/TeV	Log	$0.1 \sim 1.0$	$\tilde{m}_{\tilde{\mu}_R}$/TeV	Log	$0.1 \sim 1.0$
$m_S'^2$/TeV^2	Flat	$-1.0 \sim 1.0$			

Table 4. Parameter space explored in this study. Other dimensional parameters not crucial to this study are fixed at 3 TeV, including the SUSY parameters for the first and third generation sleptons, three generation squarks (except for A_t and A_b with the assumption $A_b = A_t$), and gluinos. All the parameters are defined at the renormalization scale $Q = 1$ TeV.

direct search for extra Higgs bosons at LEP, Tevatron, and LHC and the fit of h's property to LHC Higgs data are implemented by the programmes `HiggsBounds-5.3.2` [162–165] and `HiggsSignal-2.2.3` [166–169], respectively.

3.1 Research strategy

The `MultiNest` algorithm [111] is employed to scan comprehensively the parameter space in table 4. The $n_{\rm live}$ parameter in the algorithm controls the number of active points sampled in each iteration of the scan, and $n_{\rm live} = 8000$ is set. The following likelihood function is constructed to guide the scan:

$$\mathcal{L} = \mathcal{L}_{a_\mu} \times \mathcal{L}_{\rm const}, \tag{3.1}$$

where $\mathcal{L}_{a_\mu}$ is the likelihood function of the muon $g-2$ anomaly given by

$$\mathcal{L}_{a_\mu} \equiv {\rm Exp}\left[-\frac{1}{2}\left(\frac{a_\mu^{\rm SUSY} - \Delta a_\mu}{\delta a_\mu}\right)^2\right] = {\rm Exp}\left[-\frac{1}{2}\left(\frac{a_\mu^{\rm SUSY} - 2.51\times10^{-9}}{5.9\times10^{-10}}\right)^2\right],$$

with $\Delta a_\mu \equiv a_\mu^{\rm Exp} - a_\mu^{\rm SM}$ and δa_μ denoting the difference between the experimental central value of a_μ and its SM prediction, and the total uncertainties in determining Δa_μ, respectively [5–27]. $\mathcal{L}_{\rm const}$ represents the impacts of experimental constraints on the theory: $\mathcal{L}_{\rm const} = 1$ by our definition if the constraints are satisfied and $\mathcal{L}_{\rm const} = {\rm Exp}[-100]$ if they are not. These constraints include 2σ bounds of the DM relic density [170], upper bounds of the XENON-1T experiment on the DM-nucleon scattering [92, 93], consistence of h's property with the LHC Higgs data at 95% confidence level [169], collider searches for extra Higgs bosons [165], 2σ bounds on the branching ratios of $B \to X_s\gamma$ and $B_s \to \mu^+\mu^-$ [171], and the vacuum stability of the scalar potential consisting of the Higgs fields and the last two generation slepton fields [172, 173]. In refs. [68, 81], we presented the details of these constraints. We emphasize one subtle thing about the prior distributions: if a log

JHEP03(2023)198

distribution is adopted for $\mu_{\rm eff}$, more than 80% of the samples obtained in the scan predict a singlino-dominated $\tilde{\chi}_1^0$, while if a flat distribution is adopted, nearly all the samples correspond to a bino-dominated $\tilde{\chi}_1^0$. The reason is as follows: a small λ of $\mathcal{O}(10^{-2})$ is favorite by the singlino-dominated DM to suppress the DM-nucleon scattering, and given $\mu_{\rm eff} \equiv \lambda v_s/\sqrt{2}$ with $v_s \sim \mathcal{O}(1\,\text{TeV})$, the typical size of $\mu_{\rm eff}$ is around several tens of GeV. We verified that there is no such a phenomenon for the other parameters. We also verified that if the log distributions in table 4 are replaced by flat distributions and the region of $\mu_{\rm eff} \leq 1\,\text{TeV}$ by $\mu_{\rm eff} \leq 30\,\text{GeV}$, a renewed scan of the parameter space can reproduce the crucial characteristics of the dark gray and royal blue points in figures 1 and 2.

Next, only the samples predicting a singlino-dominated DM and satisfying all the constraints are investigated. The following processes are studied to decide whether they pass the constraints from the LHC search for SUSY or not:

$$pp \to \tilde{\chi}_i^0 \tilde{\chi}_j^{\pm}, \qquad i = 2,3,4,5, \quad j = 1,2; \tag{3.2}$$

$$pp \to \tilde{\chi}_i^{\pm} \tilde{\chi}_j^{\mp}, \quad i,j = 1,2; \tag{3.3}$$

$$pp \to \tilde{\chi}_i^0 \tilde{\chi}_j^0, \quad i,j = 2,3,4,5; \tag{3.4}$$

$$pp \to \tilde{\mu}_i^* \tilde{\mu}_j, \quad i,j = 1,2; \tag{3.5}$$

$$pp \to \tilde{\nu}_\mu^* \tilde{\nu}_\mu. \tag{3.6}$$

Specifically, the cross-sections of these processes at $\sqrt{s} = 13\,\text{TeV}$ are calculated at the next-to-leading order (NLO) by the package `Prospino2` [174]. In order to save computing time, the program `SModelS-2.1.1` [175] is initially used to exclude the obtained samples. Given that this program's capability to implement the LHC constraints is limited by its database and strict working prerequisites, the surviving samples are further surveyed by simulating the analyses in tables 1 and 2. This study is accomplished by the following steps: 60000 and 40000 events are generated for the electroweakino and slepton production processes, respectively, by package `MadGraph_aMC@NLO` [176, 177]; relevant parton shower and hadronization are finished by program `PYTHIA8` [178]; the resulting event files are then fed into package `CheckMATE-2.0.29` [179–181] to calculate the R-value defined by $R \equiv max\{S_i/S_{i,obs}^{95}\}$, where S_i denotes the simulated event number of the i-th SR in the analyses of tables 1 and 2, and $S_{i,obs}^{95}$ represents its corresponding 95% confidence level upper limit. Note that program `Delphes` is encoded in the CheckMATE for detector simulation [182].

3.2 Key features of the results

We first study the DM physics of the GNMSSM comparatively. In the Z_3-NMSSM, the DM candidate is bino-dominated in most cases, and it obtains the measured relic density mainly by co-annihilating with wino-dominated electroweakinos or the sleptons with the left-handed chirality as their dominant components. This conclusion is reflected in figures 2 and 3 of ref. [82], where we studied the Z_3-NMSSM similarly to this work, and projected the obtained samples onto $|m_{\tilde{\chi}_1^0}| - m_{\tilde{\chi}_1^\pm}$ and $|m_{\tilde{\chi}_1^0}| - m_{\tilde{\mu}_L}$ planes ($m_{\tilde{\chi}_1^\pm}$ and $m_{\tilde{\mu}_L}$ denote the

JHEP03(2023)198

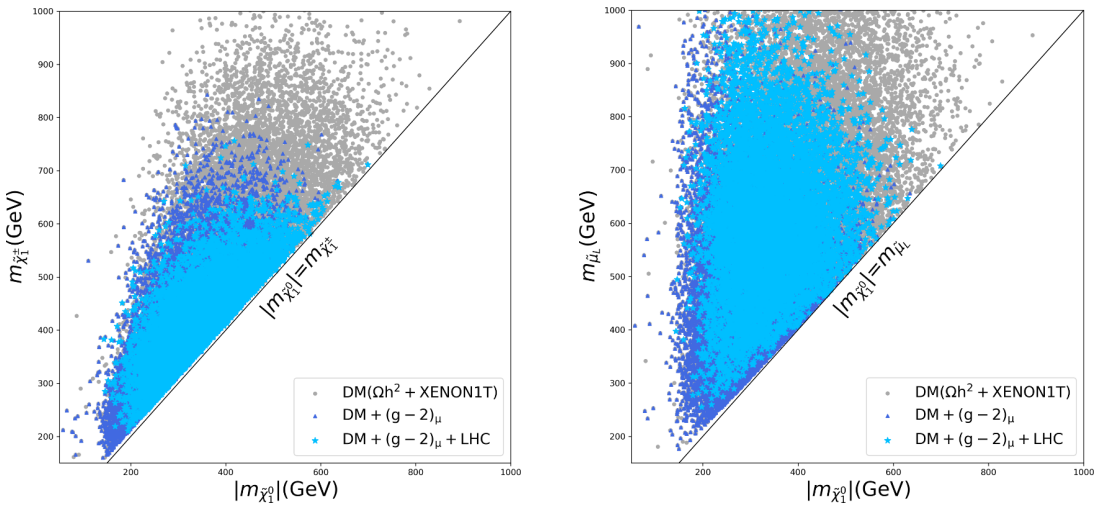

Figure 1. Projection of the obtained samples onto the $|m_{\tilde{\chi}_1^0}| - m_{\tilde{\chi}_1^\pm}$ plane (left panel) and the $|m_{\tilde{\chi}_1^0}| - m_{\tilde{\mu}_L}$ plane (right panel). The dark grey points denote the samples that satisfy all constraints listed in the text, in particular those from the DM experiments. The royal blue triangles represent those that can further explain the muon g-2 anomaly at 2σ level, and the sky blue stars are part of the royal blue triangles which agree with the results from the LHC search for SUSY.

mass of the lightest chargino and the left-handed dominant smuon, respectively).[6] Here we project the samples of this study onto the same planes to obtain figure 1. Evidently, this figure differs significantly from the corresponding ones in ref. [82] by that only a small portion of the samples predict $m_{\tilde{\chi}_1^\pm} \simeq |m_{\tilde{\chi}_1^0}|$ or $m_{\tilde{\mu}_L} \simeq |m_{\tilde{\chi}_1^0}|$, which is the necessary condition for the co-annihilations. To further clarify this point, we categorize the obtained samples by their dominant annihilation mechanisms and count the number of samples in each category. We present the results in table 5. This table shows that for most of the samples, the DM annihilates mainly by $\tilde{\chi}_1^0\tilde{\chi}_1^0 \to h_s h_s, h_s A_s$ to obtain the measured relic density, which coincides with the analyses in section 2. Figure 1 and table 5 also indicate

[6] In Bayesian statistics, the parameter space of new physics theory is described by the posterior probability density function (PDF), which is determined by the likelihood function of the research object, the prior distributions of input parameters, and the considered parameter space [183]. In the simplest case, where all the inputs are initially assumed to be flatly distributed, the posterior PDF is proportional to the likelihood function and achieves its maximum when the theory predicts the central values of experimental measurements. For the scan done in the last subsection, its sample number within a hypercube of the parameter space is proportional to the hypercube's Bayesian evidence, acquired by integrating the PDF over the hypercube [183]. So, if the PDF of a scenario is sizable only within very narrow corners of the parameter space, it is hardly encountered in the scan by the MultiNest algorithm, and its corresponding samples are rare [111]. The fundamental reason is that the parameters of this scenario need to be finely tuned to meet relevant experimental results. In the Z_3-NMSSM, DM may be singlino-dominated, and it achieves the measured density either through co-annihilating with the higgsino-dominated electroweakinos or through the h_s- or A_s-funnel, as we recapitulated in section 1. In addition, the bino-dominated DM in both MSSM and Z_3-NMSSM may achieve the measured density by Z- or h-funnel [107, 184–192]. These scenarios, however, become more and more finely tuned after considering the improved DM direct detection experiments, which we explained in section 1. They are usually missed in the scan and, thus, of less interest when one aims to capture the global characteristics of the Z_3-NMSSM.

JHEP03(2023)198

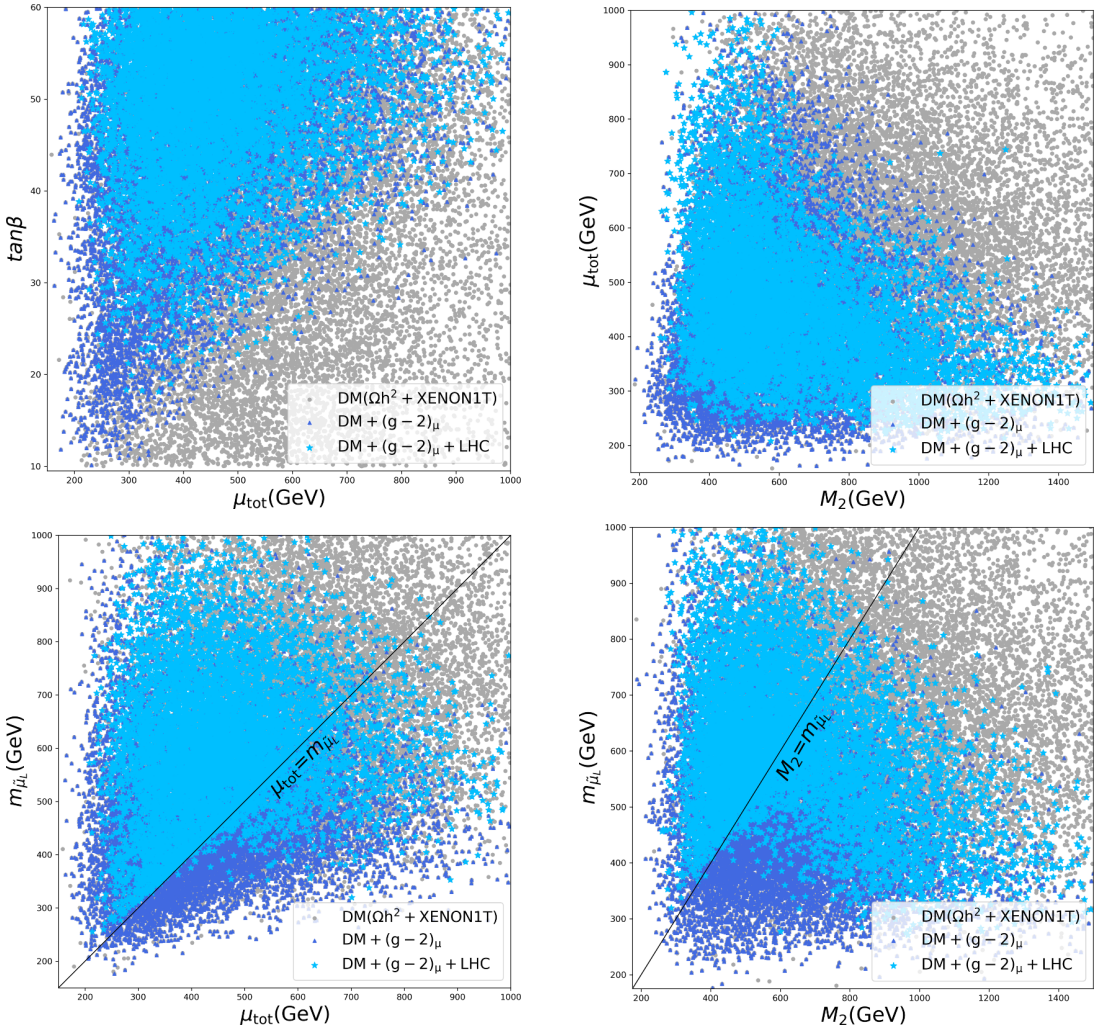

Figure 2. Similar to figure 1, but showing the correlations of the parameters that the muon g-2 is sensitive to.

that the LHC constraints are rather strong and they exclude about 59% of the obtained samples. As a result, the lower bound of $|m_{\tilde{\chi}_1^0}|$ for the samples is lifted from about 50 GeV to about 140 GeV by the constraints.[7] By contrast, we concluded in [82] that about 66% of the obtained samples are excluded if the bino-dominated DM in the Z_3-NMSSM is concerned, and $|m_{\tilde{\chi}_1^0}|$ must be larger than about 260 GeV after considering the constraints. The fundamental reason for these phenomena is at least two-fold. One is that explaining the muon g-2 anomaly requires more than one sparticle to be moderately light [79], which

[7] As explained in footnote 6, the samples obtained in this study depend strongly on the likelihood function in eq. (3.1). The statement in the text is based on the assumption that the DM is fully responsible for the measured density. If it is relaxed by setting an upper bound on the density, more parameter spaces will open, and the GNMSSM's phenomenology becomes more complicated. In this case, the lower bound of $|m_{\tilde{\chi}_1^0}|$ may be significantly reduced, and its exact value is determined only through a renewed study. This issue, however, is beyond the scope of this study. In addition, we remind that the same arguments can be applied to the conclusions in ref. [82].

JHEP03(2023)198

Annihilation Mechanisms	Without LHC Constraints	With LHC Constraints
Total Samples	20889	8517
$\tilde{\chi}_1^0\tilde{\chi}_1^0 \to h_s h_s$	10925	4028
$\tilde{\chi}_1^0\tilde{\chi}_1^0 \to h_s A_s$	8792	4115
$\tilde{\chi}_1^0\tilde{\chi}_1^0 \to h A_s$	66	18
A_s-funnel	310	62
$\tilde{\chi}_1^0\tilde{\chi}_1^0 \to A_s A_s$	6	0
$\tilde{\chi}_1^0\tilde{\chi}_1^0 \to h h_s$	2	0
Higgsino co-annihilation	385	227
Wino co-annihilation	85	61
$\tilde{\nu}_\mu/\tilde{\mu}_L$ co-annihilation	286	5
$\tilde{\mu}_R$ co-annihilation	32	1
h_s- or A_s-funnel	0	0
$Z-$ or h-funnel	0	0

Table 5. Number of the samples obtained in the scan, which are categorized by the DM dominant annihilation mechanisms and whether the LHC restrictions are considered or not. The total numbers of the royal blue triangles and the sky blue stars in figure 1 are 20889 and 8517, respectively, which are listed on the first row.

can strengthen the SUSY signals at the LHC. The other is as the DM becomes lighter, more missing transverse energy is to be emitted from the sparticle productions at the LHC, which can improve the exclusion capability of the experimental analyses.

Next, we focus on the explanation of the muon g-2 anomaly. Since the 'WHL' contribution dominates over the other ones, we show the correlations of any two of the three parameters, $\mu_{\rm tot}$, M_2, and $m_{\tilde{\mu}_L}$ in figure 2. We also plot the correlation between $\mu_{\rm tot}$ and $\tan\beta$. This figure reveals the following facts:

- The muon g-2 anomaly and the observables in DM physics may prefer different parameter spaces of the GNMSSM, but moderately broad parameter regions can still accommodate both. For example, if one requires the theory to explain the anomaly at 2σ confidence level, $\mu_{\rm tot}$, M_2, and $m_{\tilde{\mu}_L}$ must be less than about 1000 GeV, 1500 GeV, and 1000 GeV, respectively. These upper bounds depend strongly on the value of $\tan\beta$, e.g., they are about 350 GeV, 550 GeV, and 400 GeV, respectively, for $\tan\beta = 10$, and become about 800 GeV, 1100 GeV, and 800 GeV for $\tan\beta = 30$.[8] By contrast, the DM physics is not sensitive to the four parameters.

- As any one of $\mu_{\rm tot}$, M_2, and $m_{\tilde{\mu}_L}$ increases, the other two parameters tend to decrease. In other words, these three parameters can not be very large simultaneously in

[8]Note that the bounds will shrink significantly if one requires the theory to explain the anomaly at 1σ level. In this case, we find $\mu_{\rm tot} \lesssim 650$ GeV, $M_2 \lesssim 900$ GeV, and $m_{\tilde{\mu}_L} \lesssim 650$ GeV for $\tan\beta = 30$.

JHEP03(2023)198

explaining the muon g-2 anomaly. This characteristic makes the LHC restrictions on the theory rather strong.

- There are two cases that the LHC restrictions are particularly strong. One is characterized by $\tan\beta \lesssim 20$, where the winos, the higgsinos, and the left-handed dominant smuon are all lighter than about 500 GeV. This feature is shown in the top left panel for parameter $\mu_{\rm tot}$. The other case is characterized by predicting a $\tilde{\mu}_L$ lighter than winos and/or higgsinos, where the heavy electroweakinos may decay into the slepton first and thus enhance the leptonic signal of the electroweakino pair production processes (compared with the case that $\tilde{\mu}_L$ is heavier than the electroweakinos). This feature accounts for the wedge-shaped region on $M_2 - m_{\tilde{\mu}_L}$ plane, which is displayed by the LHC limits in the bottom right panel. We elaborate on this point by fixing $m_{\tilde{\mu}_L} = 350\,{\rm GeV}$ in the following. For $M_2 \lesssim 350\,{\rm GeV}$, although the wino pair production cross-sections exceed 300 fb [193, 194], there are still few samples surviving the LHC constraints. We verified that it is due to small mass splittings of the wino-like particles with $\tilde{\chi}_1^0$, where the wino-like particles decay into $\tilde{\chi}_1^0$ and a soft virtual Z or W. In the case of $350\,{\rm GeV} \lesssim M_2 \lesssim 600\,{\rm GeV}$, all the samples are excluded by the SUSY searches. This is because the wino-like particles are copiously produced at the LHC since they are moderately light, and simultaneously the branching ratios of their decays into the slepton are sizable. Specifically, we find that the ratios are always larger than 10% and may reach 60% in the optimum cases. With the further increase of M_2, the wino pair production rates rapidly decrease. Consequently, the LHC constraints are weakened, which is reflected by the frequent appearance of sky blue points in the bottom right panel. We add that this discussion can be applied to the $\mu_{\rm tot} - m_{\tilde{\mu}_L}$ plane in the bottom left panel.

- The LHC restrictions have required $\tan\beta \gtrsim 18$, $\mu_{\rm tot} \gtrsim 210\,{\rm GeV}$, $M_2 \gtrsim 260\,{\rm GeV}$, $m_{\tilde{\mu}_L} \gtrsim 255\,{\rm GeV}$, and $m_{\tilde{\mu}_R} \gtrsim 240\,{\rm GeV}$. We emphasize that moderately light higgsinos are experimentally allowed in explaining the muon g-2 anomaly. This is one of the advantages of the GNMSSM over the MSSM and the Z_3-NMSSM.

Finally, we concentrate on the particle mass spectra shown in figure 3. After comparing the normalized mass distributions before and after including the LHC restrictions (corresponding to left and right sides of the violin for each particle), one can infer that the LHC search for SUSY affects little the shape of $m_{\tilde{\chi}_{4,5}^0}$ and $m_{\tilde{\chi}_2^\pm}$ distributions, but prefers clearly more massive $\tilde{\chi}_1^0$, $\tilde{\chi}_1^\pm$, $\tilde{\chi}_2^0$, $\tilde{\chi}_3^0$, and $\tilde{\mu}_{L,R}$. The favored mass range for the latter set of particles is $140\,{\rm GeV} \lesssim m_{\tilde{\chi}_1^0} \lesssim 600\,{\rm GeV}$, $200\,{\rm GeV} \lesssim m_{\tilde{\chi}_2^0}, m_{\tilde{\chi}_1^\pm} \lesssim 700\,{\rm GeV}$, $250\,{\rm GeV} \lesssim m_{\tilde{\chi}_3^0} \lesssim 900\,{\rm GeV}$, and $255\,{\rm GeV} \lesssim m_{\tilde{\mu}_L} \lesssim 1000\,{\rm GeV}$, where the upper bounds come from the requirement to explain the muon g-2 anomaly [79]. We verify that $\tilde{\chi}_{2,3}^0$ and $\tilde{\chi}_1^\pm$ are higgsino-dominated in most cases. Figure 3 also indicates $140\,{\rm GeV} \lesssim m_{h_s} \lesssim 550\,{\rm GeV}$ and $10\,{\rm GeV} \lesssim m_{A_s} \lesssim 850\,{\rm GeV}$. These mass regions are favored by natural electroweak symmetry breaking. They also enable the scalars to play a crucial role in the DM annihilations.

JHEP03(2023)198

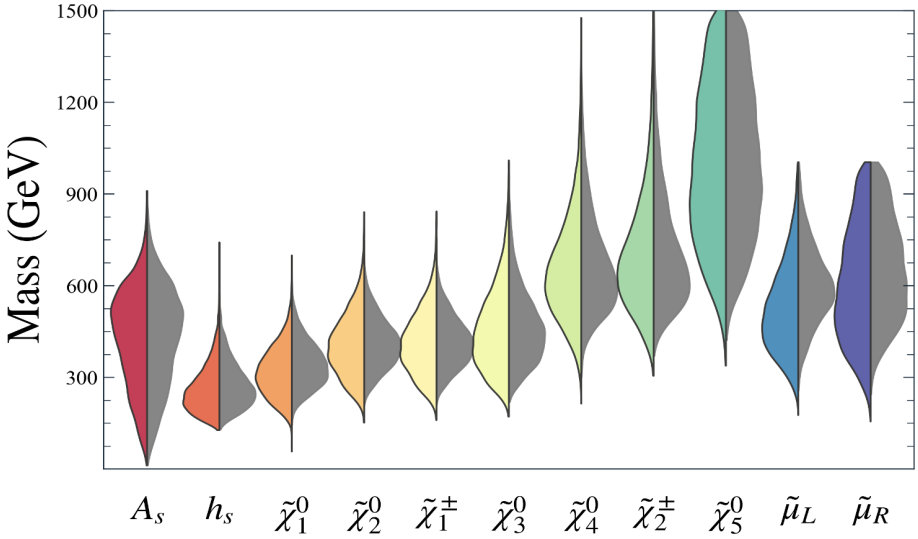

Figure 3. Split violin plot showing the mass distributions of the particles beyond the SM. This figure is plotted by counting the number of the samples obtained in the scan. The left colorful side and the right gray side of each violin are based on 20889 and 8517 samples, respectively, which are marked by the royal blue triangle and the sky blue star in figure 1. The widths of both sides are fixed so that the ratio of the two widths does not represent the relative sample number.

3.3 Impact of the LZ experiment

In the last section, the XENON-1T results were used to set upper bounds on the SI and SD cross-sections of the DM-nucleon scattering [92, 93]. These limitations, however, have been improved significantly by the recent LZ experiment [84]. So in this section, we study the impact of the LZ restrictions on the status of the GNMSSM. Specifically, we utilize the LZ results to further select the samples obtained in the last section, project them onto various panels, and compare the resulting figures with their corresponding ones in the last section. We conclude that the only difference comes from the distribution of λ: if the XENON-1T experiment is used to limit the parameter space, λ is upper bounded by about 0.09, while if the LZ constraints are adopted, it is less than 0.06.[9] This difference is shown in figure 4, where the samples are projected onto the $\lambda - \kappa$ planes. It arises from the facts that the cross-sections of the DM-nucleon scattering are proportional to λ^4 [96], and a small λ hardly affects the other observables. Due to the difference, the number of the total samples in figure 1 is reduced by a factor of about 2. In table 6, we list the distribution of the remaining samples by the DM annihilation mechanisms in analogue to table 5. This table shows similar features to table 5. In particular, both tables show that the LHC restrictions are most efficient in excluding the slepton co-annihilation cases, and least efficient in limiting the electroweakino co-annihilation cases. We explained this phenomenon in [81].

[9]The distributions of the other parameters are quite similar to those in the last section. In particular, the mass spectra distributions in figure 3 are only slightly changed.

JHEP03(2023)198

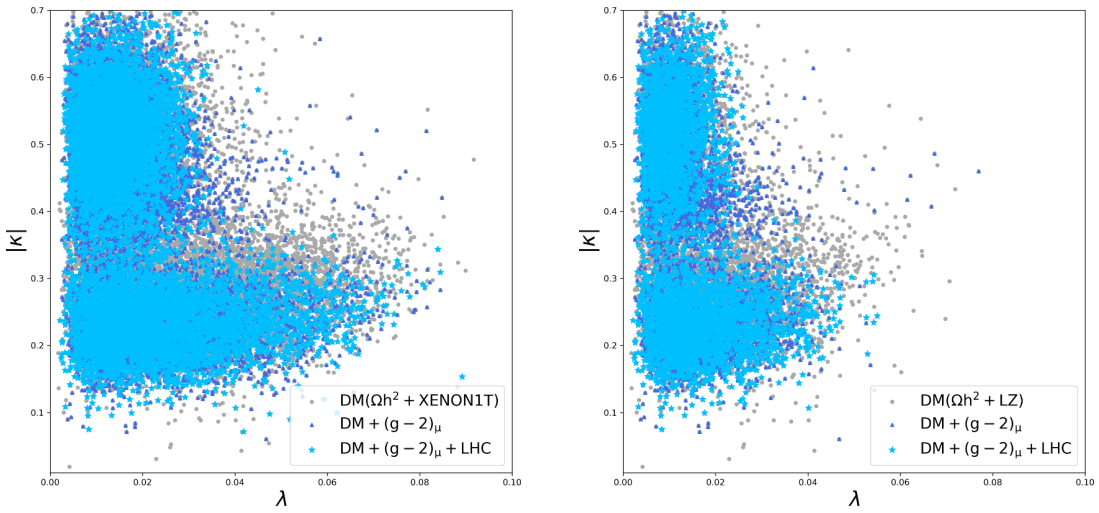

Figure 4. Left panel: similar to figure 1, but the samples are projected onto the $\lambda - |\kappa|$ plane. Right panel: same as the left panel, but it is for the samples satisfying the LZ constraints.

Annihilation Mechanisms	Without LHC Constraints	With LHC Constraints
Total Samples	9694	4166
$\tilde{\chi}_1^0\tilde{\chi}_1^0 \to h_s h_s$	4553	2207
$\tilde{\chi}_1^0\tilde{\chi}_1^0 \to h_s A_s$	4545	1736
$\tilde{\chi}_1^0\tilde{\chi}_1^0 \to h A_s$	4	0
A_s-funnel	128	37
$\tilde{\chi}_1^0\tilde{\chi}_1^0 \to A_s A_s$	3	0
$\tilde{\chi}_1^0\tilde{\chi}_1^0 \to h h_s$	1	0
Higgsino co-annihilation	235	142
Wino co-annihilation	55	41
$\tilde{\nu}_\mu/\tilde{\mu}_L$ co-annihilation	158	3
$\tilde{\mu}_R$ co-annihilation	12	0

Table 6. Same as table 5, except that the considered samples satisfy the LZ constraints.

At this stage, we emphasize several points about the LHC search for SUSY:

- There are at least two reasons why the LHC restrictions are so strong in excluding the samples. One is that we include many experimental analyses in this study, and each of them usually defines several signal regions. As a result, some of these analyses are complementary in surveying/restricting SUSY signals even when the same set of experimental data are studied. The other is explaining the muon g-2 anomaly requires more than one moderately light sparticle, which is particularly so if $\tan\beta$ is small. Consequently, the signals of different sparticles superimpose to strengthen their detection at the LHC.

JHEP03(2023)198

- Throughout this study, both the theoretical uncertainties incurred by the simulations and the experimental (systematic and statistical) uncertainties are not considered. Although these effects can relax the LHC restrictions, it is expected that much more stringent constraints on the GNMSSM will be obtained in the near future, given the advent of the high-luminosity LHC.

- In some unification theories, $\tilde{\tau}$ may be the next lightest supersymmetric particle (NLSP) due to its larger Yukawa coupling than the first-two-generation sleptons. In this case, heavy sparticles may decay into $\tilde{\tau}$ to change the production rate of the e/μ signals. Consequently, the LHC constraints can be relaxed [42]. We will discuss such a possibility in future works.

3.4 Benchmark points

In this section, we provide four parameter points in tables 7 and 8 to improve understanding the intrinsic physics. These points satisfy all the experimental constraints and exhibit the following common characteristics:

- The higgsino mass $\mu_{\rm tot}$ is less than 400 GeV so that the Z-boson mass is naturally predicted. As introduced in section 1, the MSSM does not have this property.

- The singlino-dominated DM achieves the measured relic density either by the s-wave dominated process $\tilde{\chi}_1^0\tilde{\chi}_1^0 \to h_s A_s$ or by the p-wave dominated process $\tilde{\chi}_1^0\tilde{\chi}_1^0 \to h_s h_s$. Since the annihilation cross-section of the s-wave process does not depend on DM velocity at leading order, while that of the p-wave process is proportional to v^2, different values of κ, namely $|\kappa| \sim 0.25$ and $|\kappa| \sim 0.45$, respectively, are needed for the density. In addition, a small λ around 0.01 ensures the suppression of the DM-nucleon scattering, and $v_s \lesssim 1$ TeV is compatible with natural electroweak symmetry breaking.

- Depending on M_1 and M_2, the higgsino-dominated $\tilde{\chi}_2^0$ and $\tilde{\chi}_1^\pm$ may be approximately degenerate in mass [54]. In this case, these particles will decay directly into $\tilde{\chi}_1^0$ since there are no other lighter sparticles. On the other hand, the mass splitting of $\tilde{\chi}_2^0$ and $\tilde{\chi}_3^0$ may reach 10 GeV. If the decay $\tilde{\chi}_3^0 \to \tilde{\chi}_1^0 Z$ is kinematically forbidden, the branching ratios of $\tilde{\chi}_3^0 \to \tilde{\chi}_2^0 Z^* \to \tilde{\chi}_2^0 f\bar{f}$ and $\tilde{\chi}_3^0 \to \tilde{\chi}_1^0 Z^* \to \tilde{\chi}_1^0 f\bar{f}$ are comparable since they are all three-body decays. While if $\tilde{\chi}_3^0 \to \tilde{\chi}_1^0 Z$ is kinematically accessible, the branching ratio of $\tilde{\chi}_3^0 \to \tilde{\chi}_2^0 Z^* \to \tilde{\chi}_2^0 f\bar{f}$ is usually negligibly small.

- For the other heavy sparticles, they tend to decay first into the lighter sparticles other than $\tilde{\chi}_1^0$ given the singlet nature of $\tilde{\chi}_1^0$. As a result, their decay chain is rather complex.

- A massive $\tilde{\chi}_1^0$ is utilized to suppress the $E_T^{\rm miss}$ in SUSY signals, and at the same time, massive $\tilde{\mu}_{L,R}$ are adopted to suppress slepton production rates. These mechanisms are helpful for the points to keep consistent with the LHC data.

JHEP03(2023)198

Benchmark Point P1				Benchmark Point P2			
λ	0.018	m_{h_s}	246.0 GeV	λ	0.01	m_{h_s}	215.2 GeV
κ	-0.22	m_{A_s}	100.0 GeV	κ	0.48	m_{A_s}	532.6 GeV
$\tan\beta$	29.0	m_h	125.4 GeV	$\tan\beta$	29.8	m_h	124.8 GeV
μ	330.7 GeV	m_H	1444.7 GeV	μ	318.9 GeV	m_H	1351.4 GeV
μ_{tot}	336.6 GeV	m_{A_H}	1444.7 GeV	μ_{tot}	320.2 GeV	m_{A_H}	1351.4 GeV
A_t	2544.2 GeV	$m_{\tilde{\chi}_1^0}$	-271.1 GeV	A_t	2389.2 GeV	$m_{\tilde{\chi}_1^0}$	237.9 GeV
A_κ	-192.1 GeV	$m_{\tilde{\chi}_2^0}$	333.7 GeV	A_κ	266.8 GeV	$m_{\tilde{\chi}_2^0}$	315.9 GeV
M_1	-1251.4 GeV	$m_{\tilde{\chi}_3^0}$	-347.5 GeV	M_1	1137.0 GeV	$m_{\tilde{\chi}_3^0}$	-332.3 GeV
M_2	565.0 GeV	$m_{\tilde{\chi}_4^0}$	605.9 GeV	M_2	564.8 GeV	$m_{\tilde{\chi}_4^0}$	604.8 GeV
$\tilde{m}_{\tilde{\mu}_L}$	630.0 GeV	$m_{\tilde{\chi}_5^0}$	-1255.9 GeV	$\tilde{m}_{\tilde{\mu}_L}$	623.6 GeV	$m_{\tilde{\chi}_5^0}$	1141.1 GeV
$\tilde{m}_{\tilde{\mu}_R}$	997.9 GeV	$m_{\tilde{\chi}_1^\pm}$	336.2 GeV	$\tilde{m}_{\tilde{\mu}_R}$	868.0 GeV	$m_{\tilde{\chi}_1^\pm}$	320.2 GeV
a_μ^{SUSY}	1.34×10^{-9}	$m_{\tilde{\chi}_2^\pm}$	606.2 GeV	a_μ^{SUSY}	1.46×10^{-9}	$m_{\tilde{\chi}_2^\pm}$	605.3 GeV
Ωh^2	0.12	$m_{\tilde{\mu}_L}$	635.9 GeV	Ωh^2	0.13	$m_{\tilde{\mu}_L}$	631.6 GeV
σ_p^{SI}	1.83×10^{-47}cm^2	$m_{\tilde{\mu}_R}$	1002.7 GeV	σ_p^{SI}	1.71×10^{-47}cm^2	$m_{\tilde{\mu}_R}$	873.2 GeV
σ_n^{SD}	1.44×10^{-45}cm^2	$m_{\tilde{\nu}_\mu}$	630.7 GeV	σ_n^{SD}	1.07×10^{-46}cm^2	$m_{\tilde{\nu}_\mu}$	626.3 GeV
$N_{11}, N_{12}, N_{13}, N_{14}, N_{15}$	0.0011, 0.0021, 0.0186, 0.0237, -0.9995			$N_{11}, N_{12}, N_{13}, N_{14}, N_{15}$	0.0006, -0.0028, 0.0093, -0.0121, 0.9999		
$N_{21}, N_{22}, N_{23}, N_{24}, N_{25}$	-0.019, -0.216, 0.701, -0.679, -0.004			$N_{21}, N_{22}, N_{23}, N_{24}, N_{25}$	0.037, -0.202, 0.705, -0.679, -0.015		
$N_{31}, N_{32}, N_{33}, N_{34}, N_{35}$	0.033, 0.058, 0.703, 0.707, 0.030			$N_{31}, N_{32}, N_{33}, N_{34}, N_{35}$	-0.020, 0.059, 0.702, 0.710, 0.002		
$N_{41}, N_{42}, N_{43}, N_{44}, N_{45}$	-0.005, 0.975, 0.114, -0.193, -0.0004			$N_{41}, N_{42}, N_{43}, N_{44}, N_{45}$	0.015, -0.006, 0.103, -0.183, -0.0005		
$N_{51}, N_{52}, N_{53}, N_{54}, N_{55}$	0.999, -0.002, -0.009, -0.037, 2.54E-05			$N_{51}, N_{52}, N_{53}, N_{54}, N_{55}$	0.999, -0.006, -0.014, 0.043, -8.42E-06		
Annihilations	Fractions[%]			Annihilations	Fractions[%]		
$\tilde{\chi}_1^0\tilde{\chi}_1^0 \to h_s A_s / h_s h_s$	96.0/3.1			$\tilde{\chi}_1^0\tilde{\chi}_1^0 \to h_s h_s$	99.6		
Decays	Branching ratios[%]			Decays	Branching ratios[%]		
$\tilde{\chi}_2^0 \to \tilde{\chi}_1^0 Z^\star (\to f\bar{f})$	100			$\tilde{\chi}_2^0 \to \tilde{\chi}_1^0 Z^\star (\to f\bar{f})$	100		
$\tilde{\chi}_3^0 \to \tilde{\chi}_2^0 Z^\star / \tilde{\chi}_1^0 Z^\star / \tilde{\chi}_1^\pm W^{\mp\star}$	39.5/39.3/21.2			$\tilde{\chi}_3^0 \to \tilde{\chi}_1^0 Z / \tilde{\chi}_2^0 Z^\star / \tilde{\chi}_1^\pm W^{\mp\star}$	77.4/14.4/8.2		
$\tilde{\chi}_4^0 \to \tilde{\chi}_1^\pm W^\mp / \tilde{\chi}_3^0 Z / \tilde{\chi}_2^0 h / \tilde{\chi}_2^0 Z / \tilde{\chi}_3^0 h$	55.4/22.0/19.5/1.9/1.1			$\tilde{\chi}_4^0 \to \tilde{\chi}_1^\pm W^\mp / \tilde{\chi}_3^0 Z / \tilde{\chi}_2^0 h / \tilde{\chi}_2^0 Z / \tilde{\chi}_3^0 h$	56.3/21.4/18.8/2.1/1.3		
$\tilde{\chi}_5^0 \to \tilde{\chi}_1^\pm W^\mp / \tilde{\nu}_\mu \nu_\mu / \tilde{\mu}_L^\pm \mu^\mp / \tilde{\mu}_R^\pm \mu^\mp / \tilde{\chi}_3^0 h / \tilde{\chi}_4^0 h / \tilde{\chi}_3^0 Z / \tilde{\chi}_2 h / \tilde{\chi}_4^0 Z$	25.1/16.1/15.7/15.0/9.9/9.0/3.6/3.6/3.3			$\tilde{\chi}_5^0 \to \tilde{\chi}_1^\pm W^\mp / \tilde{\mu}_R^\pm \mu^\mp / \tilde{\nu}_\mu \nu_\mu / \tilde{\mu}_L^\pm \mu^\mp / \tilde{\chi}_3^0 Z / \tilde{\chi}_2^0 h / \tilde{\chi}_2^\pm W^\mp / \tilde{\chi}_2^0 Z / \tilde{\chi}_2^0 Z$	22.9/18.9/13.7/12.9/10.7/9.7/3.2/2.9/2.7		
$\tilde{\chi}_1^\pm \to \tilde{\chi}_1^0 W^{\pm\star}$	100			$\tilde{\chi}_1^\pm \to \tilde{\chi}_1^0 W^\pm$	100		
$\tilde{\chi}_2^\pm \to \tilde{\chi}_2^0 W^\pm / \tilde{\chi}_3^0 W^\pm / \tilde{\chi}_1^\pm Z / \tilde{\chi}_1^\pm h$	26.9/25.8/25.6/21.7			$\tilde{\chi}_2^\pm \to \tilde{\chi}_2^0 W^\pm / \tilde{\chi}_3^0 W^\pm / \tilde{\chi}_1^\pm Z / \tilde{\chi}_1^\pm h$	26.3/25.8/25.7/22.1		
$\tilde{\mu}_L^\pm \to \tilde{\chi}_2^0 \mu^\pm / \tilde{\chi}_1^\pm \nu_\mu / \tilde{\chi}_2^\pm \nu_\mu / \tilde{\chi}_4^0 \mu^\pm / \tilde{\chi}_3^0 \mu^\pm$	33.4/33.1/19.7/9.8/4.0			$\tilde{\mu}_L^\pm \to \tilde{\chi}_1^\pm \nu_\mu / \tilde{\chi}_2^0 \mu^\pm / \tilde{\chi}_2^\pm \nu_\mu / \tilde{\chi}_4^0 \mu^\pm / \tilde{\chi}_3^0 \mu^\pm$	37.7/29.3/20.1/10.4/2.5		
$\tilde{\mu}_R^\pm \to \tilde{\chi}_3^0 \mu^\pm / \tilde{\chi}_1^\pm \nu_\mu / \tilde{\chi}_2^0 \mu^\pm / \tilde{\nu}_\mu W^\pm / \tilde{\mu}_L^\pm h / \tilde{\mu}_L^\pm Z$	40.3/29.1/23.6/2.5/1.2/1.2			$\tilde{\mu}_R^\pm \to \tilde{\chi}_2^0 \mu^\pm / \tilde{\chi}_1^\pm \nu_\mu / \tilde{\chi}_3^0 \mu^\pm / \tilde{\nu}_\mu W^\pm / \tilde{\chi}_4^0 \mu^\pm / \tilde{\mu}_L^\pm h$	43.5/26.9/22.5/2.2/2.1/1.0		
$\tilde{\nu}_\mu \to \tilde{\chi}_1^\pm \mu^\mp / \tilde{\chi}_2^0 \nu_\mu / \tilde{\chi}_2^\pm \mu^\mp / \tilde{\chi}_4^0 \nu_\mu$	66.7/18.7/9.1/4.9			$\tilde{\nu}_\mu \to \tilde{\chi}_1^\pm \mu^\mp / \tilde{\chi}_2^0 \nu / \tilde{\chi}_2^\pm \mu^\mp / \tilde{\chi}_4^0 \nu_\mu / \tilde{\chi}_3^0 \nu_\mu$	64.3/23.2/6.8/3.6/2.2		
R value	0.48, ATLAS-2106-01676			R value	0.51, CMS-SUS-16-039		

Table 7. Detailed information of two benchmark points, P1 and P2, that are consistent with all experimental data. These two points are characterized by a moderately large $\tan\beta$.

JHEP03(2023)198

Benchmark Point P3				Benchmark Point P4			
λ	0.012	m_{h_s}	248.6 GeV	λ	0.005	m_{h_s}	216.5 GeV
κ	0.25	m_{A_s}	162.2 GeV	κ	-0.44	m_{A_s}	314.8 GeV
$\tan\beta$	51.3	m_h	125.2 GeV	$\tan\beta$	55.4	m_h	125.5 GeV
μ	384.4 GeV	m_H	2235.7 GeV	μ	343.1 GeV	m_H	2077.0 GeV
μ_{tot}	393.1 GeV	m_{A_H}	2235.7 GeV	μ_{tot}	344.4 GeV	m_{A_H}	2077.0 GeV
A_t	2540.9 GeV	$m_{\tilde{\chi}_1^0}$	271.8 GeV	A_t	2533.8 GeV	$m_{\tilde{\chi}_1^0}$	-237.5 GeV
A_κ	-112.1 GeV	$m_{\tilde{\chi}_2^0}$	402.4 GeV	A_κ	47.0 GeV	$m_{\tilde{\chi}_2^0}$	346.8 GeV
M_1	-854.6 GeV	$m_{\tilde{\chi}_3^0}$	-404.3 GeV	M_1	796.9 GeV	$m_{\tilde{\chi}_3^0}$	-358.0 GeV
M_2	1267.9 GeV	$m_{\tilde{\chi}_4^0}$	-858.8 GeV	M_2	826.3 GeV	$m_{\tilde{\chi}_4^0}$	801.0 GeV
$\tilde{m}_{\tilde{\mu}_L}$	390.0 GeV	$m_{\tilde{\chi}_5^0}$	1303.3 GeV	$\tilde{m}_{\tilde{\mu}_L}$	580.1 GeV	$m_{\tilde{\chi}_5^0}$	864.4 GeV
$\tilde{m}_{\tilde{\mu}_R}$	569.7 GeV	$m_{\tilde{\chi}_1^\pm}$	403.5 GeV	$\tilde{m}_{\tilde{\mu}_R}$	715.4 GeV	$m_{\tilde{\chi}_1^\pm}$	351.5 GeV
a_μ^{SUSY}	1.42×10^{-9}	$m_{\tilde{\chi}_2^\pm}$	1303.5 GeV	a_μ^{SUSY}	2.15×10^{-9}	$m_{\tilde{\chi}_2^\pm}$	864.2 GeV
Ωh^2	0.11	$m_{\tilde{\mu}_L}$	405.4 GeV	Ωh^2	0.13	$m_{\tilde{\mu}_L}$	591.8 GeV
σ_p^{SI}	$1.67\times10^{-47}\text{cm}^2$	$m_{\tilde{\mu}_R}$	575.1 GeV	σ_p^{SI}	$1.36\times10^{-47}\text{cm}^2$	$m_{\tilde{\mu}_R}$	720.2 GeV
σ_n^{SD}	$7.52\times10^{-47}\text{cm}^2$	$m_{\tilde{\nu}_\mu}$	397.4 GeV	σ_n^{SD}	$4.68\times10^{-48}\text{cm}^2$	$m_{\tilde{\nu}_\mu}$	586.2 GeV
$N_{11}, N_{12}, N_{13}, N_{14}, N_{15}$	-0.0004, -0.0007, 0.0064, -0.0095, 0.9999			$N_{11}, N_{12}, N_{13}, N_{14}, N_{15}$	-0.0002, 0.0003, 0.0031, 0.0047, -0.9999		
$N_{21}, N_{22}, N_{23}, N_{24}, N_{25}$	0.025, 0.063, -0.708, 0.703, 0.011			$N_{21}, N_{22}, N_{23}, N_{24}, N_{25}$	-0.068, -0.109, 0.709, -0.693, -0.001		
$N_{31}, N_{32}, N_{33}, N_{34}, N_{35}$	-0.067, -0.032, -0.706, -0.705, -0.002			$N_{31}, N_{32}, N_{33}, N_{34}, N_{35}$	-0.026, 0.045, 0.703, 0.709, 0.005		
$N_{41}, N_{42}, N_{43}, N_{44}, N_{45}$	0.997, -0.003, -0.030, -0.065, -1.33E-05			$N_{41}, N_{42}, N_{43}, N_{44}, N_{45}$	-0.993, -0.099, 0.026, -0.056, -3.93E-06		
$N_{51}, N_{52}, N_{53}, N_{54}, N_{55}$	0.001, -0.998, -0.022, 0.067, 4.3E-06			$N_{51}, N_{52}, N_{53}, N_{54}, N_{55}$	0.091, -0.988, -0.049, 0.115, 3.82E-05		
Annihilations	Fractions[%]			Annihilations	Fractions[%]		
$\tilde{\chi}_1^0\tilde{\chi}_1^0 \to h_s A_s/h_s h_s/A_s A_s$	91.8/6.4/1.7			$\tilde{\chi}_1^0\tilde{\chi}_1^0 \to h_s h_s/hA_s/h_s A_s$	96.8/2.7/1.7/1.4		
Decays	Branching ratios[%]			Decays	Branching ratios[%]		
$\tilde{\chi}_2^0 \to \tilde{\chi}_1^0 h/\tilde{\chi}_1^0 Z/\tilde{\nu}_\mu\nu_\mu$	83.9/14.5/1.6			$\tilde{\chi}_2^0 \to \tilde{\chi}_1^0 Z$	100		
$\tilde{\chi}_3^0 \to \tilde{\chi}_1^0 Z$	99.6			$\tilde{\chi}_3^0 \to \tilde{\chi}_1^0 Z/\tilde{\chi}_2^0 Z^\star$	96.3/3.1		
$\tilde{\chi}_4^0 \to \tilde{\mu}_R^\pm\mu^\mp/\tilde{\chi}_1^\pm W^\mp/\tilde{\nu}_\mu\nu_\mu/\tilde{\mu}_L^\pm\mu^\mp/\tilde{\chi}_3^0 h/\tilde{\chi}_2^0 Z/\tilde{\chi}_3^0 Z/\tilde{\chi}_2^0 h$	29.2/20.6/15.0/14.4/9.2/8.8/1.4/1.2			$\tilde{\chi}_4^0 \to \tilde{\chi}_1^\pm W^\mp/\tilde{\mu}_L^\pm\mu^\mp/\tilde{\chi}_3^0 Z/\tilde{\chi}_2^0 h/\tilde{\mu}_R^\pm\mu^\mp/\tilde{\nu}_\mu\nu_\mu/\tilde{\chi}_2^0 Z/\tilde{\chi}_3^0 h$	50.2/12.1/11.1/10.7/6.2/6.2/1.6/1.5		
$\tilde{\chi}_5^0 \to \tilde{\chi}_1^\pm W^\mp/\tilde{\nu}_\mu\nu_\mu/\tilde{\mu}_L^\pm\mu^\mp/\tilde{\chi}_2^0 h/\tilde{\chi}_3^0 Z/\tilde{\chi}_2 Z/\tilde{\chi}_3^0 h$	27.3/22.7/22.4/10.7/10.7/2.8/2.7			$\tilde{\chi}_5^0 \to \tilde{\chi}_1^\pm W^\mp/\tilde{\chi}_3^0 Z/\tilde{\chi}_2^0 h/\tilde{\nu}_\mu\nu_\mu/\tilde{\mu}_L^\pm\mu^\mp/\tilde{\chi}_3^0 Z/\tilde{\chi}_2^0 Z$	35.8/17.9/16.7/13.1/10.2/3.1/2.7		
$\tilde{\chi}_1^\pm \to \tilde{\chi}_1^0 W^\pm/\tilde{\nu}_\mu\mu^\pm$	93.3/6.7			$\tilde{\chi}_1^\pm \to \tilde{\chi}_1^0 W^\pm$	100		
$\tilde{\chi}_2^\pm \to \tilde{\nu}_\mu\mu^\pm/\tilde{\mu}_L^\pm\nu_\mu/\tilde{\chi}_3^0 W^\pm/\tilde{\chi}_2^0 W^\pm/\tilde{\chi}_1^\pm Z/\tilde{\chi}_1^\pm h$	22.3/22.3/13.6/13.6/13.5/13.5			$\tilde{\chi}_2^\pm \to \tilde{\chi}_3^0 W^\pm/\tilde{\chi}_1^\pm Z/\tilde{\chi}_2^0 W^\pm/\tilde{\chi}_1^\pm h/\tilde{\nu}_\mu\mu^\pm/\tilde{\mu}_L^\pm\nu_\mu$	19.5/19.3/19.0/18.6/11.7/11.5		
$\tilde{\mu}_L^\pm \to \tilde{\chi}_2^0\mu^\pm/\tilde{\chi}_1^0\mu^\pm/\tilde{\chi}_1^\pm\nu_\mu$	71.0/13.5/6.6			$\tilde{\mu}_L^\pm \to \tilde{\chi}_1^\pm\nu_\mu/\tilde{\chi}_2^0\mu^\pm/\tilde{\chi}_2^\pm\nu_\mu/\tilde{\chi}_3^0\mu^\pm$	41.3/40.5/18.2		
$\tilde{\mu}_R^\pm \to \tilde{\chi}_3^0\mu^\pm/\tilde{\chi}_1^\pm\nu_\mu/\tilde{\nu}_\mu W^\pm/\tilde{\chi}_2^0\mu^\pm/\tilde{\mu}_L^\pm h/\tilde{\mu}_L^\pm Z$	33.2/22.7/16.5/14.5/7.0/6.1			$\tilde{\mu}_R^\pm \to \tilde{\chi}_2^0\mu^\pm/\tilde{\chi}_1^\pm\nu_\mu/\tilde{\chi}_3^0\mu^\pm$	45.3/30.9/20.2		
$\tilde{\nu}_\mu \to \tilde{\chi}_1^0\nu_\mu$	100			$\tilde{\nu}_\mu \to \tilde{\chi}_1^\pm\mu^\mp/\tilde{\chi}_2^0\nu_\mu/\tilde{\chi}_3^0\nu_\mu$	67.9/27.8/4.3		
R value	0.18, CMS-SUS-16-039			R value	0.62, ATLAS-2106-01676		

Table 8. Detailed information of another two benchmark points, P3 and P4, satisfying all experimental constraints. These two points are characterized by a large $\tan\beta$.

The four points differ mainly in how to further suppress the ratio R. Specifically, points P1 and P2 predict $\tan\beta < 30$ so that M_2 should be moderately small to explain the muon g-2 anomaly. Since the wino-dominated $\tilde{\chi}_4^0$ and $\tilde{\chi}_2^\pm$ are copiously produced at the LHC, their decay into $\tilde{\mu}_{L,R}$ must be kinematically forbidden. Otherwise, the probability of $\tilde{\chi}_4^0$ and $\tilde{\chi}_2^\pm$ decaying into leptonic final states will be enhanced by mediating an on-shell $\tilde{\mu}_{L/R}$, which can significantly increase the R-value. In addition, the compressed mass spectra, $\mu_{\rm tot} - m_{\tilde{\chi}_1^0} < m_Z$, are helpful to suppress the signals of the higgsino-dominated electroweakinos. By contrast, points P3 and P4 correspond to $\tan\beta > 50$, and M_2 may be exceedingly large in explaining the muon g-2 anomaly. Given the productions of the wino-dominated electroweakinos are suppressed by their large masses, they can not contribute to R significantly even when their decays into $\tilde{\mu}_{L,R}$ are open.

Finally, we add that the samples marked by the sky blue stars in figure 1 will be explored at future colliders given that they predict some moderately light sparticles, in particular $m_{\tilde{\chi}_1^0}, m_{\tilde{\chi}_2^0}, m_{\tilde{\chi}_1^\pm} \lesssim 700\,\text{GeV}$. This issue was discussed in refs. [67, 75, 79, 195]. It was found that, although only a part of the preferred parameter space can be covered at the high luminosity LHC, an exhaustive coverage of the parameter space is possible at a high-energy e^+e^- collider with $\sqrt{s} \gtrsim 1\,\text{TeV}$, such as ILC with $\sqrt{s} = 1\,\text{TeV}$ [196] and CLIC with $\sqrt{s} = 1\,\text{TeV}$ [197, 198]. This conclusion was shown in figure 4 of [195], where the capability of different colliders to probe the explanation of the muon g-2 anomaly was compared for the bino-wino co-annihilation case.

3.5 More discussions of the results

We explain more about the results of this work.

1. The $a_\mu^{\rm SM}$ used currently by the theory initiative includes only the computations published before 2020 in its officially released results and does not reflect the more recent determinations on the lattice with small errors [7, 28]. As suggested by the recent lattice simulation of the BMW collaboration on the hadronic vacuum polarization (HVP) contribution to a_μ [28], the muon g-2 anomaly may arise from the uncertainties in calculating the hadronic contribution to the moment. If this speculation is corroborated in the future, $a_\mu^{\rm SUSY}$ should be much smaller than its currently favored size, and any of the electroweakinos and $\tilde{\mu}_{L/R}$ are not necessarily light. In this case, the LHC restrictions on sparticle mass spectra will be relaxed significantly. For example, we updated the results of ref. [96], which only studied the DM physics in GNMSSM, by including the recent LZ constraints. We found that the SUSY searches in table 1 only excluded about 4% of the remaining samples in figure 2 of ref. [96].

2. As introduced in section 2.4, the search for charginos and neutralinos using fully hadronic final states of W/Z and Higgs bosons can be more potent in excluding SUSY parameter points than the leptonic signal analysis included in this study. It occurs when the wino-like particles are heavier than about 600 GeV, their mass splitting with $\tilde{\chi}_1^0$ is larger than about 300 GeV, and $m_{\tilde{\chi}_1^0} \lesssim 400\,\text{GeV}$. We study the sky blue samples in the right panel of figure 4 that satisfy these conditions and have the following observations:

JHEP03(2023)198

- Winos are heavier than higgsinos alone for about 4% of the samples, and they are heavier than both higgsinos and $\tilde{\mu}_R$ for another 8% of the samples. Since mass splittings between the winos and the higgsinos are always larger than 100 GeV, the branching ratios of winos decaying into higgsinos are characterized by $Br(\tilde{W} \to \tilde{H}W^{\pm}) \gtrsim 50\%$, $Br(\tilde{W} \to \tilde{H}Z) < 25\%$, and $Br(\tilde{W} \to \tilde{H}h) < 25\%$ ($\tilde{W}$ and $\tilde{H}$ denote the wino-dominated particles and the higgsino-dominated particles, respectively),[10] which is shown in table 7 for benchmark points P1 and P2. In the higgsino co-annihilation case, the higgsinos are approximately degenerate with the singlino-dominated DM in mass and are regarded as missing momentum in the hadronic analysis [1]. In this case, one can estimate the R-values. Assuming $Br(\tilde{W} \to \tilde{H}W^{\pm}) = 50\%$, $Br(\tilde{W} \to \tilde{H}Z) = 25\%$, and $Br(\tilde{W} \to \tilde{H}h) = 25\%$, and noting that the chargino pair production rate at the LHC is about one-half of the chargino-neutralino associated production rate, we conclude that the R-values of our case are acquired by rescaling those in figure 15 of ref. [1], with a factor of 0.75, 0.375, and 0.375 for the $W^{\pm}W^{\mp}$, $W^{\pm}Z$, and $W^{\pm}h$ signal, respectively. In addition, as suggested by the results of the hadronic analysis [1], the mass splitting between the winos and the higgsinos should be larger than about 400 GeV to boost the decay products W/Z and h, which can facilitate their detection using large-radius jets and jet substructure information. We utilize this criterion to refine the two types of samples and find their total percentage is reduced from 12% to 0.7%, indicating that the hadronic analysis may have exclusion capability only for a small portion of the samples. We emphasize that the rescalings further reduce this capability.
- Regarding the rest 88% of the samples, we find that winos are always heavier than higgsinos and $\tilde{\mu}_L$. In this case, the wino-like particles may decay into the left-handed dominated sleptons. The branching ratios exceed 20% and may reach 60% in the optimum case. This characteristic is shown in table 8 for benchmark points P3 and P4. As a result, the branching ratios of the decays into W/Z and h are suppressed as the new channels open up, which can further reduce the capability of the hadronic signals in the SUSY search.

We note that the latest version of the SModelS, namely SModelS-2.2.1 [199], has included the cut efficiency of the hadronic analysis, and it contains some signal topologies that can be applied to some samples of this study. We utilize this code to further refine the sky blue samples in the right panel of figure 4. We find that it has no exclusion capability. We plan to supplement the hadronic analysis into the package CheckMATE to carefully study its impact on SUSY parameter space in our future research project.

Based on the discussions, we conclude that the hadronic analysis is not crucial to the heavy wino case of this study because the decay branching ratios into Z and h are suppressed significantly and also because the momentums of W/Z and h tend to be soft in the cascade decay of the wino-like particles when compared with the scenario

[10] Note that the wino decay modes in the two cases are similar because the strength of wino couplings to $\tilde{\mu}_R$ is much weaker than that to the higgsinos.

JHEP03(2023)198

NLSP Type	W/O LHC Cons.	W/ LHC Cons.	SRs and their exclusion percentages
Total	9694	4166	SR-1(24.5%), SR-2(14.3%), SR-3(6.8%), SR-4(5.1%)
Higgsino	5003	2934	SR-1(25.4%), SR-2(5.3%), SR-4(4.5%), SR-5(2.5%)
$\tilde{\nu}_\mu$	2147	174	SR-2(39.6%), SR-3(26.7%), SR-1(8.3%), SR-5(8.3%)
Wino	1246	951	SR-1(9.4%), SR-2(8.9%), SR-5(2.6%), SR-6(1.9%)
$\tilde{\mu}_{\rm R}$	1013	18	SR-1(62.7%), SR-2(17.6%), SR-4(8.8%), SR-3(4.9%)
Bino	285	89	SR-1(55.2%), SR-2(6.2%), SR-4(4.1%), SR-5(2.1%)

Table 9. Numbers of the royal blue samples in the right panel of figure 4, categorized by the NLSP's dominant component and whether the LHC restrictions are considered, are presented in the first three columns of the table, respectively. In the fourth column, we list the SRs that contribute to the largest R-values and their capability to exclude the scenarios in terms of the percentage of the total numbers in the second column. This table indicates that the LHC restriction on the wino-dominated NLSP scenario is relatively weak, while that on the $\tilde{\mu}_R$ NLSP scenario is very strong. We explained this phenomenon in refs. [68, 81]. This table also indicates that the experimental analyses in ref. [133] are usually most potent in excluding the samples.

that the particles directly decay into $\tilde{\chi}_1^0$. We add that these mechanisms to suppress the capability of the hadronic signal in SUSY search also work in the heavy higgsino case. Furthermore, this case has another distinct characteristic: since winos are usually significantly lighter than 600 GeV when $\mu_{\rm tot} \gtrsim 600\,{\rm GeV}$ (see the upper right panel of figure 2), wino production rate is much larger than the higgsino rate, which is less than 10 fb for $\mu_{\rm tot} = 600\,{\rm GeV}$ [193, 194]. In such a situation, it is evident that the leptonic analysis is more favored to exclude the samples.

3. As introduced before, heavy sparticle prefers to decay first into lighter ones other than the LSP. Its decay chain is rather complex, and its final decay products usually contain more than one SM particle. To simplify our discussion of the LHC restrictions, we classify the royal blue samples in the right panel of figure 4 by their NLSP's dominant component, which may be any of higgsino fields, wino field, bino field, left-handed slepton field, and right-handed slepton field. Given that the critical characteristics of these scenarios and their underlying physics have been analyzed in our recent works [68, 81], we only reveal more details about the exclusion capability of the SUSY searches at the LHC. In table 9, we show sample numbers of these scenarios before and after considering the LHC restrictions, the SRs that contribute to the largest R-values, and their capability to exclude the scenarios, expressed in terms of the percentage of the total numbers in the second column. The following SRs are involved:

   - SR-1: signal regions G03, G04, and G05 defined in ref. [133]. They correspond to the LHC search for electroweakinos which focused on the events with $p_{\rm T}^{\rm miss} > 100\,{\rm GeV}$ ($p_{\rm T}^{\rm miss}$ denotes missing transverse momentum) and four or more leptons that form at least two opposite-sign same-flavor (OSSF) pairs.
   - SR-2: signal regions A44, A14, A30, and so on defined in ref. [133]. They arise from the LHC search for electroweakinos by the final state containing missing transverse momentum and three electrons or muons that form at least one OSSF pair.

JHEP03(2023)198

- SR-3: signal regions SS15, SS14, and SS12 in ref. [133]. They are designed in the LHC search for electroweakinos by the final state containing two same-sign (SS) dileptons with $p_{\mathrm{T}} > 100\,\mathrm{GeV}$ and $M_{\mathrm{T}} > 100\,\mathrm{GeV}$, and no jets.
- SR-4: signal regions SR_WZoff_high_njd, SR_incWZoff_high_njc1, SR_WZ off_high_nje, and so on defined in ref. [112]. They study the chargino-neutralino associated production at the LHC by the final state containing three leptons and missing transverse momentum, where the chargino and neutralino decay into off-shell W and Z bosons, respectively.
- SR-5: signal regions $\mathrm{S}-\mathrm{high}-\mathrm{mm}-10$, $\mathrm{S}-\mathrm{high}-\mathrm{mm}-05$, $\mathrm{E}-\mathrm{high}\ -\mathrm{mm}-30$, and so on proposed in ref. [144]. They consider the electroweakinos with compressed mass spectra and investigate their production at the LHC by the final state containing two leptons and missing transverse momentum.
- SR-6: signal regions SR_Wh_SFOS_11, SR_WZ_20, SR_Wh_SFOS_16, and so on defined in ref. [112]. They correspond to the LHC search for chargino-neutralino associated production by the final state containing three leptons and missing transverse momentum, where the chargino decays into an on-shell W boson, and the neutralino decays into an on-shell Z boson or an on-shell SM Higgs boson.

In rare cases, the following SRs are also crucial:

- SR-7: signal regions SRG08_0j_mll and SRG07_0j_mll defined in ref. [131]. They come from the LHC search for Slepton pair production, focusing on the final state containing only two OSSF leptons, and missing transverse momentum.
- SR-8: signal regions SR1_weakino_2media_mll_2 and SR1_weakino_3high_ mll_2 defined in ref. [132]. They arise from the LHC search for new physics by the signal containing two soft oppositely charged leptons and missing transverse momentum.

We add that the details of these SRs were presented in corresponding experimental reports. They are helpful to understand the results in table 9.

4 Summary

In the past decade, DM direct detection experiments have improved their sensitivity to the cross-sections of DM-nucleon scattering by more than 10^3 times [84, 92, 93, 200]. Consequently, some economical realizations of SUSY, such as the MSSM and the Z_3-NMSSM, are becoming more and more difficult to keep consistent with the experimental results in a natural way [88]. In particular, the attractiveness of the popular bino-dominated DM in these models is fading. In this context, the singlino-dominated DM in the GNMSSM arouses the researchers' interest [96]. This theory has the following distinct features [68]: free from the tadpole problem and the domain-wall problem of the Z_3-NMSSM, capable of forming an economical secluded DM sector to yield the DM experimental results naturally, and readily weaken the restrictions from the LHC search for SUSY. In addition, it predicts more stable vacuums than the Z_3-NMSSM. As a result, the theory can explain the muon

JHEP03(2023)198

g-2 anomaly in broad parameter space that agrees with all experimental results while simultaneously breaking the electroweak symmetry naturally.

In this study, we are inspired by the rapid progress of particle physics experiments in recent years and investigate how the GNMSSM coincides with various experimental data. We are particularly interested in the SUSY search at the LHC, the DM search by the LZ experiment, and the improved measurement of the muon g-2 since they can provide valuable information about SUSY. In order to survey the theory's status, we employ the MultiNest algorithm to scan elaborately its parameter space. We adopt the muon g-2 observable to guide the scan and consider the restrictions from the LHC Higgs data, the DM experimental results, the B-physics measurements, and the vacuum stability. Then, we examine the samples obtained from the scan by the LHC analyses in sparticle search. Our study reveals three spectacular features of the theory. The first is that there exist lower bounds on sparticle mass spectra, e.g., $\mu_{\rm tot} \gtrsim 210\,{\rm GeV}$, $M_2 \gtrsim 260\,{\rm GeV}$, $m_{\tilde{\chi}_1^0} \gtrsim 140\,{\rm GeV}$, $m_{\tilde{\chi}_2^0}, m_{\tilde{\chi}_1^\pm} \gtrsim 200\,{\rm GeV}$, $m_{\tilde{\chi}_3^0} \gtrsim 250\,{\rm GeV}$, $m_{\tilde{\mu}_L} \gtrsim 255\,{\rm GeV}$, and $m_{\tilde{\mu}_R} \gtrsim 240\,{\rm GeV}$. These bounds are significantly lower than those for the bino-dominated DM case in the Z_3-NMSSM [82], but far beyond the reach of the LEP experiments in searching for SUSY. They originate from the following facts: if $\tilde{\chi}_1^0$ is lighter, more missing transverse energy will be emitted in the sparticle production processes at the LHC, which can improve the sensitivities of the experimental analyses; while if the sparticles other than $\tilde{\chi}_1^0$ are lighter, they will be more copiously produced at the LHC to increase the events containing multiple leptons. The second feature is that the singlet-dominated $\tilde{\chi}_1^0$, h_s, and A_s form a secluded DM sector. Such a theoretical structure is natural in the sense that the masses of these particles can be regarded as free parameters, and all of them and v_s are at the weak scale. The relic density can be obtained either by the s-wave dominated annihilation $\tilde{\chi}_1^0\tilde{\chi}_1^0 \to h_s A_s$ with $|\kappa| \sim 0.25$ or by the p-wave dominated annihilation $\tilde{\chi}_1^0\tilde{\chi}_1^0 \to h_s h_s$ with $|\kappa| \sim 0.45$. The last feature is that the improving detections of the DM-nucleon scattering influence the theory only by preferring a smaller and smaller λ, which is currently upper bounded by about 0.05. Since the 'visible' sector (in comparison with the DM sector) is scarcely affected, one does not need to worry about the drastic change of the theory's phenomenology if the scattering rate is found below the neutrino floor. Evidently, our study provides a simple and clear picture of the physics inherent in the GNMSSM, although it possesses more input parameters than the MSSM and the Z_3-NMSSM.

This work extends the study in [110] by considering a more general theoretical framework and utilizing more advanced and sophisticated research strategies. As a result, the conclusions obtained in this work are more robust than those of the previous work. They exhibit the most essential characteristics of the NMSSM.

Acknowledgments

This work is supported by the National Natural Science Foundation of China (NNSFC) under grant No. 12075076.

JHEP03(2023)198

References

[1] ATLAS collaboration, *Search for charginos and neutralinos in final states with two boosted hadronically decaying bosons and missing transverse momentum in pp collisions at $\sqrt{s}$ = 13 TeV with the ATLAS detector*, *Phys. Rev. D* **104** (2021) 112010 [arXiv:2108.07586] [INSPIRE].

[2] G. Jungman, M. Kamionkowski and K. Griest, *Supersymmetric dark matter*, *Phys. Rept.* **267** (1996) 195 [hep-ph/9506380] [INSPIRE].

[3] ATLAS collaboration, *Search for new phenomena in pp collisions in final states with tau leptons, b-jets, and missing transverse momentum with the ATLAS detector*, *Phys. Rev. D* **104** (2021) 112005 [arXiv:2108.07665] [INSPIRE].

[4] ATLAS collaboration, *Search for squarks and gluinos in final states with jets and missing transverse momentum using 139 fb^{-1} of $\sqrt{s} = 13$ TeV pp collision data with the ATLAS detector*, *JHEP* **02** (2021) 143 [arXiv:2010.14293] [INSPIRE].

[5] MUON $g-2$ collaboration, *Measurement of the Positive Muon Anomalous Magnetic Moment to 0.46 ppm*, *Phys. Rev. Lett.* **126** (2021) 141801 [arXiv:2104.03281] [INSPIRE].

[6] MUON $g-2$ collaboration, *Final Report of the Muon E821 Anomalous Magnetic Moment Measurement at BNL*, *Phys. Rev. D* **73** (2006) 072003 [hep-ex/0602035] [INSPIRE].

[7] T. Aoyama et al., *The anomalous magnetic moment of the muon in the Standard Model*, *Phys. Rept.* **887** (2020) 1 [arXiv:2006.04822] [INSPIRE].

[8] T. Aoyama, M. Hayakawa, T. Kinoshita and M. Nio, *Complete Tenth-Order QED Contribution to the Muon g − 2*, *Phys. Rev. Lett.* **109** (2012) 111808 [arXiv:1205.5370] [INSPIRE].

[9] T. Aoyama, T. Kinoshita and M. Nio, *Theory of the Anomalous Magnetic Moment of the Electron*, *Atoms* **7** (2019) 28 [INSPIRE].

[10] A. Czarnecki, W.J. Marciano and A. Vainshtein, *Refinements in electroweak contributions to the muon anomalous magnetic moment*, *Phys. Rev. D* **67** (2003) 073006 [*Erratum ibid.* **73** (2006) 119901] [hep-ph/0212229] [INSPIRE].

[11] C. Gnendiger, D. Stöckinger and H. Stöckinger-Kim, *The electroweak contributions to $(g-2)_\mu$ after the Higgs boson mass measurement*, *Phys. Rev. D* **88** (2013) 053005 [arXiv:1306.5546] [INSPIRE].

[12] M. Davier, A. Hoecker, B. Malaescu and Z. Zhang, *Reevaluation of the hadronic vacuum polarisation contributions to the Standard Model predictions of the muon g − 2 and $\alpha(m_Z^2)$ using newest hadronic cross-section data*, *Eur. Phys. J. C* **77** (2017) 827 [arXiv:1706.09436] [INSPIRE].

[13] A. Keshavarzi, D. Nomura and T. Teubner, *Muon g − 2 and $\alpha(M_Z^2)$: a new data-based analysis*, *Phys. Rev. D* **97** (2018) 114025 [arXiv:1802.02995] [INSPIRE].

[14] G. Colangelo, M. Hoferichter and P. Stoffer, *Two-pion contribution to hadronic vacuum polarization*, *JHEP* **02** (2019) 006 [arXiv:1810.00007] [INSPIRE].

JHEP03(2023)198

[15] M. Hoferichter, B.-L. Hoid and B. Kubis, *Three-pion contribution to hadronic vacuum polarization*, *JHEP* **08** (2019) 137 [arXiv:1907.01556] [INSPIRE].

[16] M. Davier, A. Hoecker, B. Malaescu and Z. Zhang, *A new evaluation of the hadronic vacuum polarisation contributions to the muon anomalous magnetic moment and to $\alpha(m_Z^2)$*, *Eur. Phys. J. C* **80** (2020) 241 [*Erratum ibid.* **80** (2020) 410] [arXiv:1908.00921] [INSPIRE].

[17] A. Keshavarzi, D. Nomura and T. Teubner, *$g-2$ of charged leptons, $\alpha(M_Z^2)$, and the hyperfine splitting of muonium*, *Phys. Rev. D* **101** (2020) 014029 [arXiv:1911.00367] [INSPIRE].

[18] A. Kurz, T. Liu, P. Marquard and M. Steinhauser, *Hadronic contribution to the muon anomalous magnetic moment to next-to-next-to-leading order*, *Phys. Lett. B* **734** (2014) 144 [arXiv:1403.6400] [INSPIRE].

[19] K. Melnikov and A. Vainshtein, *Hadronic light-by-light scattering contribution to the muon anomalous magnetic moment revisited*, *Phys. Rev. D* **70** (2004) 113006 [hep-ph/0312226] [INSPIRE].

[20] P. Masjuan and P. Sanchez-Puertas, *Pseudoscalar-pole contribution to the $(g_\mu - 2)$: a rational approach*, *Phys. Rev. D* **95** (2017) 054026 [arXiv:1701.05829] [INSPIRE].

[21] G. Colangelo, M. Hoferichter, M. Procura and P. Stoffer, *Dispersion relation for hadronic light-by-light scattering: two-pion contributions*, *JHEP* **04** (2017) 161 [arXiv:1702.07347] [INSPIRE].

[22] M. Hoferichter et al., *Dispersion relation for hadronic light-by-light scattering: pion pole*, *JHEP* **10** (2018) 141 [arXiv:1808.04823] [INSPIRE].

[23] A. Gérardin, H.B. Meyer and A. Nyffeler, *Lattice calculation of the pion transition form factor with $N_f = 2+1$ Wilson quarks*, *Phys. Rev. D* **100** (2019) 034520 [arXiv:1903.09471] [INSPIRE].

[24] J. Bijnens, N. Hermansson-Truedsson and A. Rodríguez-Sánchez, *Short-distance constraints for the HLbL contribution to the muon anomalous magnetic moment*, *Phys. Lett. B* **798** (2019) 134994 [arXiv:1908.03331] [INSPIRE].

[25] G. Colangelo et al., *Longitudinal short-distance constraints for the hadronic light-by-light contribution to $(g-2)_\mu$ with large-N_c Regge models*, *JHEP* **03** (2020) 101 [arXiv:1910.13432] [INSPIRE].

[26] T. Blum et al., *Hadronic Light-by-Light Scattering Contribution to the Muon Anomalous Magnetic Moment from Lattice QCD*, *Phys. Rev. Lett.* **124** (2020) 132002 [arXiv:1911.08123] [INSPIRE].

[27] G. Colangelo et al., *Remarks on higher-order hadronic corrections to the muon $g-2$*, *Phys. Lett. B* **735** (2014) 90 [arXiv:1403.7512] [INSPIRE].

[28] S. Borsanyi et al., *Leading hadronic contribution to the muon magnetic moment from lattice QCD*, *Nature* **593** (2021) 51 [arXiv:2002.12347] [INSPIRE].

[29] P. Athron et al., *New physics explanations of a_μ in light of the FNAL muon $g-2$ measurement*, *JHEP* **09** (2021) 080 [arXiv:2104.03691] [INSPIRE].

[30] S.P. Martin and J.D. Wells, *Muon Anomalous Magnetic Dipole Moment in Supersymmetric Theories*, *Phys. Rev. D* **64** (2001) 035003 [hep-ph/0103067] [INSPIRE].

[31] F. Domingo and U. Ellwanger, *Constraints from the Muon $g-2$ on the Parameter Space of the NMSSM*, *JHEP* **07** (2008) 079 [arXiv:0806.0733] [INSPIRE].

JHEP03(2023)198

[32] T. Moroi, *The Muon anomalous magnetic dipole moment in the minimal supersymmetric standard model*, *Phys. Rev. D* **53** (1996) 6565 [*Erratum ibid.* **56** (1997) 4424] [hep-ph/9512396] [INSPIRE].

[33] W. Hollik, J.I. Illana, S. Rigolin and D. Stockinger, *One loop MSSM contribution to the weak magnetic dipole moments of heavy fermions*, *Phys. Lett. B* **416** (1998) 345 [hep-ph/9707437] [INSPIRE].

[34] P. Athron et al., *GM2Calc: Precise MSSM prediction for* $(g-2)$ *of the muon*, *Eur. Phys. J. C* **76** (2016) 62 [arXiv:1510.08071] [INSPIRE].

[35] M. Endo, K. Hamaguchi, S. Iwamoto and T. Kitahara, *Supersymmetric interpretation of the muon* $g-2$ *anomaly*, *JHEP* **07** (2021) 075 [arXiv:2104.03217] [INSPIRE].

[36] D. Stockinger, *The Muon Magnetic Moment and Supersymmetry*, *J. Phys. G* **34** (2007) R45 [hep-ph/0609168] [INSPIRE].

[37] A. Czarnecki and W.J. Marciano, *The Muon anomalous magnetic moment: A Harbinger for 'new physics'*, *Phys. Rev. D* **64** (2001) 013014 [hep-ph/0102122] [INSPIRE].

[38] J. Cao, Z. Heng, D. Li and J.M. Yang, *Current experimental constraints on the lightest Higgs boson mass in the constrained MSSM*, *Phys. Lett. B* **710** (2012) 665 [arXiv:1112.4391] [INSPIRE].

[39] Z. Kang, $H_{u,d}$*-messenger Couplings Address the* μ/B_μ *&* $A_t/m^2_{H_u}$ *Problem and* $(g-2)_\mu$ *Puzzle*, arXiv:1610.06024 [INSPIRE].

[40] B. Zhu, R. Ding and T. Li, *Higgs mass and muon anomalous magnetic moment in the MSSM with gauge-gravity hybrid mediation*, *Phys. Rev. D* **96** (2017) 035029 [arXiv:1610.09840] [INSPIRE].

[41] T.T. Yanagida and N. Yokozaki, *Muon* $g-2$ *in MSSM gauge mediation revisited*, *Phys. Lett. B* **772** (2017) 409 [arXiv:1704.00711] [INSPIRE].

[42] K. Hagiwara, K. Ma and S. Mukhopadhyay, *Closing in on the chargino contribution to the muon* $g-2$ *in the MSSM: current LHC constraints*, *Phys. Rev. D* **97** (2018) 055035 [arXiv:1706.09313] [INSPIRE].

[43] P. Cox, C. Han and T.T. Yanagida, *Muon* $g-2$ *and dark matter in the minimal supersymmetric standard model*, *Phys. Rev. D* **98** (2018) 055015 [arXiv:1805.02802] [INSPIRE].

[44] H.M. Tran and H.T. Nguyen, *GUT-inspired MSSM in light of muon* $g-2$ *and LHC results at* $\sqrt{s} = 13$ *TeV*, *Phys. Rev. D* **99** (2019) 035040 [arXiv:1812.11757] [INSPIRE].

[45] B.P. Padley, K. Sinha and K. Wang, *Natural Supersymmetry, Muon* $g-2$*, and the Last Crevices for the Top Squark*, *Phys. Rev. D* **92** (2015) 055025 [arXiv:1505.05877] [INSPIRE].

[46] A. Choudhury et al., *Muon* $g-2$ *and related phenomenology in constrained vector-like extensions of the MSSM*, *JHEP* **05** (2017) 072 [arXiv:1701.08778] [INSPIRE].

[47] N. Okada and H.M. Tran, 125 *GeV Higgs boson mass and muon* $g-2$ *in 5D MSSM*, *Phys. Rev. D* **94** (2016) 075016 [arXiv:1606.05329] [INSPIRE].

[48] X. Du and F. Wang, *NMSSM From Alternative Deflection in Generalized Deflected Anomaly Mediated SUSY Breaking*, *Eur. Phys. J. C* **78** (2018) 431 [arXiv:1710.06105] [INSPIRE].

[49] X. Ning and F. Wang, *Solving the muon* $g-2$ *anomaly within the NMSSM from generalized deflected AMSB*, *JHEP* **08** (2017) 089 [arXiv:1704.05079] [INSPIRE].

JHEP03(2023)198

[50] K. Wang, F. Wang, J. Zhu and Q. Jie, *The semi-constrained NMSSM in light of muon $g-2$, LHC, and dark matter constraints*, *Chin. Phys. C* **42** (2018) 103109 [arXiv:1811.04435] [INSPIRE].

[51] J.-L. Yang et al., *Lepton-flavor violation and two loop electroweak corrections to $(g-2)_\mu$ in the B-L symmetric SSM*, *Phys. Rev. D* **99** (2019) 015002 [arXiv:1812.03860] [INSPIRE].

[52] C.-X. Liu et al., *Higgs boson decay $h \to Z\gamma$ and muon magnetic dipole moment in the $\mu\nu$SSM*, *JHEP* **04** (2020) 002 [arXiv:2002.04370] [INSPIRE].

[53] J. Cao et al., *Anomalous muon magnetic moment in the inverse seesaw extended next-to-minimal supersymmetric standard model*, *Phys. Rev. D* **101** (2020) 095009 [arXiv:1912.10225] [INSPIRE].

[54] J. Cao et al., *Electron and muon anomalous magnetic moments in the inverse seesaw extended NMSSM*, *Phys. Rev. D* **104** (2021) 055009 [arXiv:2102.11355] [INSPIRE].

[55] W. Ke and P. Slavich, *Higgs-mass constraints on a supersymmetric solution of the muon $g-2$ anomaly*, *Eur. Phys. J. C* **82** (2022) 89 [arXiv:2109.15277] [INSPIRE].

[56] J.L. Lamborn, T. Li, J.A. Maxin and D.V. Nanopoulos, *Resolving the $(g-2)_\mu$ Discrepancy with $\mathcal{F}$-SU(5) Intersecting D-branes*, *JHEP* **11** (2021) 081 [arXiv:2108.08084] [INSPIRE].

[57] S. Li, Y. Xiao and J.M. Yang, *Constraining CP-phases in SUSY: an interplay of muon/electron $g-2$ and electron EDM*, *Nucl. Phys. B* **974** (2022) 115629 [arXiv:2108.00359] [INSPIRE].

[58] Y. Nakai, M. Reece and M. Suzuki, *Supersymmetric alignment models for $(g-2)_\mu$*, *JHEP* **10** (2021) 068 [arXiv:2107.10268] [INSPIRE].

[59] S. Li, Y. Xiao and J.M. Yang, *Can electron and muon $g-2$ anomalies be jointly explained in SUSY?*, *Eur. Phys. J. C* **82** (2022) 276 [arXiv:2107.04962] [INSPIRE].

[60] J.S. Kim, D.E. Lopez-Fogliani, A.D. Perez and R.R. de Austri, *The new $(g-2)_\mu$ and Right-Handed Sneutrino Dark Matter*, *Nucl. Phys. B* **974** (2022) 115637 [arXiv:2107.02285] [INSPIRE].

[61] Z. Li et al., *Gluino-SUGRA scenarios in light of FNAL muon $g-2$ anomaly*, *JHEP* **12** (2021) 219 [arXiv:2106.04466] [INSPIRE].

[62] W. Altmannshofer, S.A. Gadam, S. Gori and N. Hamer, *Explaining $(g-2)_\mu$ with Multi-TeV Sleptons*, *JHEP* **07** (2021) 118 [arXiv:2104.08293] [INSPIRE].

[63] H. Baer, V. Barger and H. Serce, *Anomalous muon magnetic moment, supersymmetry, naturalness, LHC search limits and the landscape*, *Phys. Lett. B* **820** (2021) 136480 [arXiv:2104.07597] [INSPIRE].

[64] M. Chakraborti, L. Roszkowski and S. Trojanowski, *GUT-constrained supersymmetry and dark matter in light of the new $(g-2)_\mu$ determination*, *JHEP* **05** (2021) 252 [arXiv:2104.04458] [INSPIRE].

[65] A. Aboubrahim, M. Klasen and P. Nath, *What the Fermilab muon $g-2$ experiment tells us about discovering supersymmetry at high luminosity and high energy upgrades to the LHC*, *Phys. Rev. D* **104** (2021) 035039 [arXiv:2104.03839] [INSPIRE].

[66] S. Iwamoto, T.T. Yanagida and N. Yokozaki, *Wino-Higgsino dark matter in MSSM from the $g-2$ anomaly*, *Phys. Lett. B* **823** (2021) 136768 [arXiv:2104.03223] [INSPIRE].

[67] M. Chakraborti, S. Heinemeyer and I. Saha, *The new "MUON G-2" result and supersymmetry*, *Eur. Phys. J. C* **81** (2021) 1114 [arXiv:2104.03287] [INSPIRE].

JHEP03(2023)198

[68] J. Cao et al., *Improved $(g-2)_\mu$ measurement and singlino dark matter in μ-term extended $\mathbb{Z}_3$-NMSSM*, *JHEP* **09** (2021) 175 [arXiv:2104.03284] [INSPIRE].

[69] W. Yin, *Muon $g-2$ anomaly in anomaly mediation*, *JHEP* **06** (2021) 029 [arXiv:2104.03259] [INSPIRE].

[70] H.-B. Zhang, C.-X. Liu, J.-L. Yang and T.-F. Feng, *Muon anomalous magnetic dipole moment in the $\mu\nu$SSM*, *Chin. Phys. C* **46** (2022) 093107 [arXiv:2104.03489] [INSPIRE].

[71] M. Ibe, S. Kobayashi, Y. Nakayama and S. Shirai, *Muon $g-2$ in Gauge Mediation without SUSY CP Problem*, *JHEP* **07** (2021) 098 [arXiv:2104.03289] [INSPIRE].

[72] C. Han, *Muon $g-2$ and CP violation in MSSM*, arXiv:2104.03292 [INSPIRE].

[73] F. Wang et al., *GUT-scale constrained SUSY in light of new muon $g-2$ measurement*, *Nucl. Phys. B* **970** (2021) 115486 [arXiv:2104.03262] [INSPIRE].

[74] M.-D. Zheng and H.-H. Zhang, *Studying the $b \to s\ell^+\ell^-$ anomalies and $(g-2)_\mu$ in R-parity violating MSSM framework with the inverse seesaw mechanism*, *Phys. Rev. D* **104** (2021) 115023 [arXiv:2105.06954] [INSPIRE].

[75] M. Chakraborti, S. Heinemeyer, I. Saha and C. Schappacher, *$(g-2)_\mu$ and SUSY dark matter: direct detection and collider search complementarity*, *Eur. Phys. J. C* **82** (2022) 483 [arXiv:2112.01389] [INSPIRE].

[76] A. Aboubrahim, M. Klasen, P. Nath and R.M. Syed, *Tests of gluino-driven radiative breaking of the electroweak symmetry at the LHC*, *Phys. Scripta* **97** (2022) 054002 [arXiv:2112.04986] [INSPIRE].

[77] M.I. Ali, M. Chakraborti, U. Chattopadhyay and S. Mukherjee, *Muon and electron $(g-2)$ anomalies with non-holomorphic interactions in MSSM*, *Eur. Phys. J. C* **83** (2023) 60 [arXiv:2112.09867] [INSPIRE].

[78] K. Wang and J. Zhu, *Smuon in the NMSSM confronted with the muon $g-2$ anomaly and SUSY searches*, *Chin. Phys. C* **47** (2023) 013107 [arXiv:2112.14576] [INSPIRE].

[79] M. Chakraborti, S. Heinemeyer and I. Saha, *Improved $(g-2)_\mu$ Measurements and Supersymmetry*, *Eur. Phys. J. C* **80** (2020) 984 [arXiv:2006.15157] [INSPIRE].

[80] S. Baum, M. Carena, N.R. Shah and C.E.M. Wagner, *The tiny $(g-2)$ muon wobble from small-μ supersymmetry*, *JHEP* **01** (2022) 025 [arXiv:2104.03302] [INSPIRE].

[81] J. Cao et al., *Impact of recent $(g-2)_\mu$ measurement on the light CP-even Higgs scenario in general Next-to-Minimal Supersymmetric Standard Model*, *JHEP* **03** (2022) 203 [arXiv:2201.11490] [INSPIRE].

[82] J. Cao et al., *Impact of LHC probes of SUSY and recent measurement of $(g-2)_\mu$ on Z_3-NMSSM*, *Sci. China Phys. Mech. Astron.* **65** (2022) 291012 [arXiv:2204.04710] [INSPIRE].

[83] F. Domingo, U. Ellwanger and C. Hugonie, *M_W, dark matter and a_μ in the NMSSM*, *Eur. Phys. J. C* **82** (2022) 1074 [arXiv:2209.03863] [INSPIRE].

[84] LZ collaboration, *First Dark Matter Search Results from the LUX-ZEPLIN (LZ) Experiment*, arXiv:2207.03764 [INSPIRE].

[85] T. Falk, K.A. Olive and M. Srednicki, *Heavy sneutrinos as dark matter*, *Phys. Lett. B* **339** (1994) 248 [hep-ph/9409270] [INSPIRE].

JHEP03(2023)198

[86] M. Chakraborti, S. Heinemeyer and I. Saha, *Improved $(g-2)_\mu$ measurements and wino/higgsino dark matter*, *Eur. Phys. J. C* **81** (2021) 1069 [arXiv:2103.13403] [INSPIRE].

[87] S. Baum, M. Carena, N.R. Shah and C.E.M. Wagner, *Higgs portals for thermal Dark Matter. EFT perspectives and the NMSSM*, *JHEP* **04** (2018) 069 [arXiv:1712.09873] [INSPIRE].

[88] J. Cao et al., *Suppressing the scattering of WIMP dark matter and nucleons in supersymmetric theories*, *Phys. Rev. D* **101** (2020) 075003 [arXiv:1910.14317] [INSPIRE].

[89] A. Pierce, N.R. Shah and K. Freese, *Neutralino Dark Matter with Light Staus*, arXiv:1309.7351 [MCTP-13-30] [INSPIRE].

[90] L. Calibbi, J.M. Lindert, T. Ota and Y. Takanishi, *LHC Tests of Light Neutralino Dark Matter without Light Sfermions*, *JHEP* **11** (2014) 106 [arXiv:1410.5730] [INSPIRE].

[91] C. Cheung et al., *NMSSM Interpretation of the Galactic Center Excess*, *Phys. Rev. D* **90** (2014) 075011 [arXiv:1406.6372] [INSPIRE].

[92] XENON collaboration, *Dark Matter Search Results from a One Ton-Year Exposure of XENON1T*, *Phys. Rev. Lett.* **121** (2018) 111302 [arXiv:1805.12562] [INSPIRE].

[93] XENON collaboration, *Constraining the spin-dependent WIMP-nucleon cross sections with XENON1T*, *Phys. Rev. Lett.* **122** (2019) 141301 [arXiv:1902.03234] [INSPIRE].

[94] H. Baer, V. Barger, P. Huang and X. Tata, *Natural Supersymmetry: LHC, dark matter and ILC searches*, *JHEP* **05** (2012) 109 [arXiv:1203.5539] [INSPIRE].

[95] H. Zhou, J. Cao, J. Lian and D. Zhang, *Singlino-dominated dark matter in Z3-symmetric NMSSM*, *Phys. Rev. D* **104** (2021) 015017 [arXiv:2102.05309] [INSPIRE].

[96] J. Cao et al., *Singlino-dominated dark matter in general NMSSM*, *JHEP* **06** (2021) 176 [arXiv:2102.05317] [INSPIRE].

[97] G. Belanger et al., *Relic density of dark matter in the NMSSM*, *JCAP* **09** (2005) 001 [hep-ph/0505142] [INSPIRE].

[98] J. Cao, H.E. Logan and J.M. Yang, *Experimental constraints on nMSSM and implications on its phenomenology*, *Phys. Rev. D* **79** (2009) 091701 [arXiv:0901.1437] [INSPIRE].

[99] F. Mahmoudi, J. Rathsman, O. Stal and L. Zeune, *Light Higgs bosons in phenomenological NMSSM*, *Eur. Phys. J. C* **71** (2011) 1608 [arXiv:1012.4490] [INSPIRE].

[100] J.-J. Cao et al., *Light dark matter in NMSSM and implication on Higgs phenomenology*, *Phys. Lett. B* **703** (2011) 292 [arXiv:1104.1754] [INSPIRE].

[101] J. Cao et al., *A light SUSY dark matter after CDMS-II, LUX and LHC Higgs data*, *JHEP* **05** (2014) 056 [arXiv:1311.0678] [INSPIRE].

[102] T. Han, Z. Liu and S. Su, *Light Neutralino Dark Matter: Direct/Indirect Detection and Collider Searches*, *JHEP* **08** (2014) 093 [arXiv:1406.1181] [INSPIRE].

[103] U. Ellwanger and A.M. Teixeira, *NMSSM with a singlino LSP: possible challenges for searches for supersymmetry at the LHC*, *JHEP* **10** (2014) 113 [arXiv:1406.7221] [INSPIRE].

[104] J. Cao et al., *Supersymmetry explanation of the Fermi Galactic Center excess and its test at LHC run II*, *Phys. Rev. D* **91** (2015) 055005 [arXiv:1410.3239] [INSPIRE].

[105] J. Cao et al., *Interpreting the galactic center gamma-ray excess in the NMSSM*, *JHEP* **10** (2015) 030 [arXiv:1506.06471] [INSPIRE].

JHEP03(2023)198

[106] W. Abdallah, A. Chatterjee and A.K. Datta, *Revisiting singlino dark matter of the natural Z_3-symmetric NMSSM in the light of LHC*, *JHEP* **09** (2019) 095 [arXiv:1907.06270] [INSPIRE].

[107] K. Wang and J. Zhu, *Funnel annihilations of light dark matter and the invisible decay of the Higgs boson*, *Phys. Rev. D* **101** (2020) 095028 [arXiv:2003.01662] [INSPIRE].

[108] R.K. Barman et al., *Current bounds and future prospects of light neutralino dark matter in NMSSM*, *Phys. Rev. D* **103** (2021) 015029 [arXiv:2006.07854] [INSPIRE].

[109] W. Ahmed, M. Goodsell and S. Munir, *Dark matter in the CP-violating NMSSM*, *Eur. Phys. J. C* **82** (2022) 539 [arXiv:2201.10628] [INSPIRE].

[110] J. Cao et al., *Current status of a natural NMSSM in light of LHC 13 TeV data and XENON-1T results*, *Phys. Rev. D* **99** (2019) 075020 [arXiv:1810.09143] [INSPIRE].

[111] F. Feroz, M.P. Hobson and M. Bridges, *MultiNest: an efficient and robust Bayesian inference tool for cosmology and particle physics*, *Mon. Not. Roy. Astron. Soc.* **398** (2009) 1601 [arXiv:0809.3437] [INSPIRE].

[112] ATLAS collaboration, *Search for chargino-neutralino pair production in final states with three leptons and missing transverse momentum in $\sqrt{s} = 13$ TeV pp collisions with the ATLAS detector*, *Eur. Phys. J. C* **81** (2021) 1118 [arXiv:2106.01676] [INSPIRE].

[113] U. Ellwanger, C. Hugonie and A.M. Teixeira, *The Next-to-Minimal Supersymmetric Standard Model*, *Phys. Rept.* **496** (2010) 1 [arXiv:0910.1785] [INSPIRE].

[114] M. Maniatis, *The Next-to-Minimal Supersymmetric extension of the Standard Model reviewed*, *Int. J. Mod. Phys. A* **25** (2010) 3505 [arXiv:0906.0777] [INSPIRE].

[115] P. Fayet, *Supergauge Invariant Extension of the Higgs Mechanism and a Model for the electron and Its Neutrino*, *Nucl. Phys. B* **90** (1975) 104 [INSPIRE].

[116] U. Ellwanger, *Nonrenormalizable interactions from supergravity, quantum corrections and effective low-energy theories*, *Phys. Lett. B* **133** (1983) 187 [INSPIRE].

[117] S.A. Abel, *Destabilizing divergences in the NMSSM*, *Nucl. Phys. B* **480** (1996) 55 [hep-ph/9609323] [INSPIRE].

[118] C.F. Kolda, S. Pokorski and N. Polonsky, *Stabilized singlets in supergravity as a source of the μ parameter*, *Phys. Rev. Lett.* **80** (1998) 5263 [hep-ph/9803310] [INSPIRE].

[119] C. Panagiotakopoulos and K. Tamvakis, *Stabilized NMSSM without domain walls*, *Phys. Lett. B* **446** (1999) 224 [hep-ph/9809475] [INSPIRE].

[120] H.M. Lee et al., *A unique $\mathbb{Z}_4^R$ symmetry for the MSSM*, *Phys. Lett. B* **694** (2011) 491 [arXiv:1009.0905] [INSPIRE].

[121] H.M. Lee et al., *Discrete R symmetries for the MSSM and its singlet extensions*, *Nucl. Phys. B* **850** (2011) 1 [arXiv:1102.3595] [INSPIRE].

[122] G.G. Ross and K. Schmidt-Hoberg, *The Fine-Tuning of the Generalised NMSSM*, *Nucl. Phys. B* **862** (2012) 710 [arXiv:1108.1284] [INSPIRE].

[123] G.G. Ross, K. Schmidt-Hoberg and F. Staub, *The Generalised NMSSM at One Loop: Fine Tuning and Phenomenology*, *JHEP* **08** (2012) 074 [arXiv:1205.1509] [INSPIRE].

[124] J.-J. Cao et al., *A SM-like Higgs near 125 GeV in low energy SUSY: a comparative study for MSSM and NMSSM*, *JHEP* **03** (2012) 086 [arXiv:1202.5821] [INSPIRE].

JHEP03(2023)198

[125] ATLAS collaboration, *Search for heavy Higgs bosons decaying into two tau leptons with the ATLAS detector using pp collisions at $\sqrt{s} = 13$ TeV*, *Phys. Rev. Lett.* **125** (2020) 051801 [arXiv:2002.12223] [INSPIRE].

[126] ATLAS collaboration, *Search for charged Higgs bosons decaying into a top quark and a bottom quark at $\sqrt{s} = 13$ TeV with the ATLAS detector*, *JHEP* **06** (2021) 145 [arXiv:2102.10076] [INSPIRE].

[127] M. Badziak, M. Olechowski and P. Szczerbiak, *Blind spots for neutralino dark matter in the NMSSM*, *JHEP* **03** (2016) 179 [arXiv:1512.02472] [INSPIRE].

[128] M. Badziak, M. Olechowski and P. Szczerbiak, *Spin-dependent constraints on blind spots for thermal singlino-higgsino dark matter with(out) light singlets*, *JHEP* **07** (2017) 050 [arXiv:1705.00227] [INSPIRE].

[129] M. Pospelov, A. Ritz and M.B. Voloshin, *Secluded WIMP Dark Matter*, *Phys. Lett. B* **662** (2008) 53 [arXiv:0711.4866] [INSPIRE].

[130] K.-M. Cheung, C.-H. Chou and O.C.W. Kong, *Muon anomalous magnetic moment, two Higgs doublet model, and supersymmetry*, *Phys. Rev. D* **64** (2001) 111301 [hep-ph/0103183] [INSPIRE].

[131] CMS collaboration, *Search for supersymmetry in final states with two oppositely charged same-flavor leptons and missing transverse momentum in proton-proton collisions at $\sqrt{s} = 13$ TeV*, *JHEP* **04** (2021) 123 [arXiv:2012.08600] [INSPIRE].

[132] CMS collaboration, *Combined search for electroweak production of charginos and neutralinos in proton-proton collisions at $\sqrt{s} = 13$ TeV*, *JHEP* **03** (2018) 160 [arXiv:1801.03957] [INSPIRE].

[133] CMS collaboration, *Search for electroweak production of charginos and neutralinos in multilepton final states in proton-proton collisions at $\sqrt{s} = 13$ TeV*, *JHEP* **03** (2018) 166 [arXiv:1709.05406] [INSPIRE].

[134] ATLAS collaboration, *Search for electroweak production of supersymmetric particles in final states with two or three leptons at $\sqrt{s} = 13$ TeV with the ATLAS detector*, *Eur. Phys. J. C* **78** (2018) 995 [arXiv:1803.02762] [INSPIRE].

[135] ATLAS collaboration, *Search for chargino-neutralino production using recursive jigsaw reconstruction in final states with two or three charged leptons in proton-proton collisions at $\sqrt{s} = 13$ TeV with the ATLAS detector*, *Phys. Rev. D* **98** (2018) 092012 [arXiv:1806.02293] [INSPIRE].

[136] ATLAS collaboration, *Search for direct production of electroweakinos in final states with one lepton, missing transverse momentum and a Higgs boson decaying into two b-jets in pp collisions at $\sqrt{s} = 13$ TeV with the ATLAS detector*, *Eur. Phys. J. C* **80** (2020) 691 [arXiv:1909.09226] [INSPIRE].

[137] ATLAS collaboration, *Search for chargino and neutralino production in final states with a Higgs boson and missing transverse momentum at $\sqrt{s} = 13$ TeV with the ATLAS detector*, *Phys. Rev. D* **100** (2019) 012006 [arXiv:1812.09432] [INSPIRE].

[138] CMS collaboration, *Search for new phenomena in final states with two opposite-charge, same-flavor leptons, jets, and missing transverse momentum in pp collisions at $\sqrt{s} = 13$ TeV*, *JHEP* **03** (2018) 076 [arXiv:1709.08908] [INSPIRE].

[139] CMS collaboration, *Search for supersymmetry with Higgs boson to diphoton decays using the razor variables at $\sqrt{s} = 13$ TeV*, *Phys. Lett. B* **779** (2018) 166 [arXiv:1709.00384] [INSPIRE].

JHEP03(2023)198

[140] ATLAS collaboration, *Search for electroweak production of charginos and sleptons decaying into final states with two leptons and missing transverse momentum in $\sqrt{s} = 13$ TeV pp collisions using the ATLAS detector*, *Eur. Phys. J. C* **80** (2020) 123 [arXiv:1908.08215] [INSPIRE].

[141] CMS collaboration, *Searches for pair production of charginos and top squarks in final states with two oppositely charged leptons in proton-proton collisions at $\sqrt{s} = 13$ TeV*, *JHEP* **11** (2018) 079 [arXiv:1807.07799] [INSPIRE].

[142] ATLAS collaboration, *Search for photonic signatures of gauge-mediated supersymmetry in 13 TeV pp collisions with the ATLAS detector*, *Phys. Rev. D* **97** (2018) 092006 [arXiv:1802.03158] [INSPIRE].

[143] ATLAS collaboration, *Search for supersymmetry in events with four or more charged leptons in 139 fb^{-1} of $\sqrt{s} = 13$ TeV pp collisions with the ATLAS detector*, *JHEP* **07** (2021) 167 [arXiv:2103.11684] [INSPIRE].

[144] ATLAS collaboration, *Searches for electroweak production of supersymmetric particles with compressed mass spectra in $\sqrt{s} = 13$ TeV pp collisions with the ATLAS detector*, *Phys. Rev. D* **101** (2020) 052005 [arXiv:1911.12606] [INSPIRE].

[145] ATLAS collaboration, *Search for electroweak production of supersymmetric states in scenarios with compressed mass spectra at $\sqrt{s} = 13$ TeV with the ATLAS detector*, *Phys. Rev. D* **97** (2018) 052010 [arXiv:1712.08119] [INSPIRE].

[146] CMS collaboration, *Search for new physics in events with two soft oppositely charged leptons and missing transverse momentum in proton-proton collisions at $\sqrt{s} = 13$ TeV*, *Phys. Lett. B* **782** (2018) 440 [arXiv:1801.01846] [INSPIRE].

[147] CMS collaboration, *Search for supersymmetric partners of electrons and muons in proton-proton collisions at $\sqrt{s} = 13$ TeV*, *Phys. Lett. B* **790** (2019) 140 [arXiv:1806.05264] [INSPIRE].

[148] P. Fayet, *Spontaneously Broken Supersymmetric Theories of Weak, Electromagnetic and Strong Interactions*, *Phys. Lett. B* **69** (1977) 489 [INSPIRE].

[149] G.R. Farrar and P. Fayet, *Phenomenology of the Production, Decay, and Detection of New Hadronic States Associated with Supersymmetry*, *Phys. Lett. B* **76** (1978) 575 [INSPIRE].

[150] F. Staub, *SARAH*, arXiv:0806.0538 [INSPIRE].

[151] F. Staub, *SARAH 3.2: Dirac Gauginos, UFO output, and more*, *Comput. Phys. Commun.* **184** (2013) 1792 [arXiv:1207.0906] [INSPIRE].

[152] F. Staub, *SARAH 4: A tool for (not only SUSY) model builders*, *Comput. Phys. Commun.* **185** (2014) 1773 [arXiv:1309.7223] [INSPIRE].

[153] F. Staub, *Exploring new models in all detail with SARAH*, *Adv. High Energy Phys.* **2015** (2015) 840780 [arXiv:1503.04200] [INSPIRE].

[154] W. Porod, *SPheno, a program for calculating supersymmetric spectra, SUSY particle decays and SUSY particle production at e^+e^- colliders*, *Comput. Phys. Commun.* **153** (2003) 275 [hep-ph/0301101] [INSPIRE].

[155] W. Porod and F. Staub, *SPheno 3.1: Extensions including flavour, CP-phases and models beyond the MSSM*, *Comput. Phys. Commun.* **183** (2012) 2458 [arXiv:1104.1573] [INSPIRE].

[156] W. Porod, F. Staub and A. Vicente, *A Flavor Kit for BSM models*, *Eur. Phys. J. C* **74** (2014) 2992 [arXiv:1405.1434] [INSPIRE].

JHEP03(2023)198

[157] G. Belanger, F. Boudjema, A. Pukhov and A. Semenov, *MicrOMEGAs: A Program for calculating the relic density in the MSSM*, *Comput. Phys. Commun.* **149** (2002) 103 [hep-ph/0112278] [INSPIRE].

[158] G. Belanger, F. Boudjema, A. Pukhov and A. Semenov, *MicrOMEGAs 2.0: A Program to calculate the relic density of dark matter in a generic model*, *Comput. Phys. Commun.* **176** (2007) 367 [hep-ph/0607059] [INSPIRE].

[159] G. Belanger, F. Boudjema, A. Pukhov and A. Semenov, *micrOMEGAs: A Tool for dark matter studies*, *Nuovo Cim. C* **033N2** (2010) 111 [arXiv:1005.4133] [INSPIRE].

[160] G. Belanger, F. Boudjema, A. Pukhov and A. Semenov, *micrOMEGAs_3: A program for calculating dark matter observables*, *Comput. Phys. Commun.* **185** (2014) 960 [arXiv:1305.0237] [INSPIRE].

[161] D. Barducci et al., *Collider limits on new physics within micrOMEGAs_4.3*, *Comput. Phys. Commun.* **222** (2018) 327 [arXiv:1606.03834] [INSPIRE].

[162] P. Bechtle et al., *HiggsBounds: Confronting Arbitrary Higgs Sectors with Exclusion Bounds from LEP and the Tevatron*, *Comput. Phys. Commun.* **181** (2010) 138 [arXiv:0811.4169] [INSPIRE].

[163] P. Bechtle et al., *HiggsBounds 2.0.0: Confronting Neutral and Charged Higgs Sector Predictions with Exclusion Bounds from LEP and the Tevatron*, *Comput. Phys. Commun.* **182** (2011) 2605 [arXiv:1102.1898] [INSPIRE].

[164] P. Bechtle et al., *HiggsBounds-4: Improved Tests of Extended Higgs Sectors against Exclusion Bounds from LEP, the Tevatron and the LHC*, *Eur. Phys. J. C* **74** (2014) 2693 [arXiv:1311.0055] [INSPIRE].

[165] P. Bechtle et al., *HiggsBounds-5: Testing Higgs Sectors in the LHC 13 TeV Era*, *Eur. Phys. J. C* **80** (2020) 1211 [arXiv:2006.06007] [INSPIRE].

[166] P. Bechtle et al., *HiggsSignals: Confronting arbitrary Higgs sectors with measurements at the Tevatron and the LHC*, *Eur. Phys. J. C* **74** (2014) 2711 [arXiv:1305.1933] [INSPIRE].

[167] O. Stål and T. Stefaniak, *Constraining extended Higgs sectors with HiggsSignals*, *PoS* **EPS-HEP2013** (2013) 314 [arXiv:1310.4039] [INSPIRE].

[168] P. Bechtle et al., *Probing the Standard Model with Higgs signal rates from the Tevatron, the LHC and a future ILC*, *JHEP* **11** (2014) 039 [arXiv:1403.1582] [INSPIRE].

[169] P. Bechtle et al., *HiggsSignals-2: Probing new physics with precision Higgs measurements in the LHC 13 TeV era*, *Eur. Phys. J. C* **81** (2021) 145 [arXiv:2012.09197] [INSPIRE].

[170] Planck collaboration, *Planck 2018 results. VI. Cosmological parameters*, *Astron. Astrophys.* **641** (2020) A6 [*Erratum ibid.* **652** (2021) C4] [arXiv:1807.06209] [INSPIRE].

[171] Particle Data Group collaboration, *Review of Particle Physics*, *Phys. Rev. D* **98** (2018) 030001 [INSPIRE].

[172] J.E. Camargo-Molina, B. O'Leary, W. Porod and F. Staub, *Vevacious: A Tool For Finding The Global Minima Of One-Loop Effective Potentials With Many Scalars*, *Eur. Phys. J. C* **73** (2013) 2588 [arXiv:1307.1477] [INSPIRE].

[173] J.E. Camargo-Molina et al., *Constraining the Natural MSSM through tunneling to color-breaking vacua at zero and non-zero temperature*, *Phys. Lett. B* **737** (2014) 156 [arXiv:1405.7376] [INSPIRE].

JHEP03(2023)198

[174] W. Beenakker, R. Hopker and M. Spira, *PROSPINO: A Program for the production of supersymmetric particles in next-to-leading order QCD*, hep-ph/9611232 [INSPIRE].

[175] C.K. Khosa et al., *SModelS Database Update v1.2.3*, *LHEP* **2020** (2020) 158 [arXiv:2005.00555] [INSPIRE].

[176] J. Alwall et al., *MadGraph 5: Going Beyond*, *JHEP* **06** (2011) 128 [arXiv:1106.0522] [INSPIRE].

[177] E. Conte, B. Fuks and G. Serret, *MadAnalysis 5, A User-Friendly Framework for Collider Phenomenology*, *Comput. Phys. Commun.* **184** (2013) 222 [arXiv:1206.1599] [INSPIRE].

[178] T. Sjöstrand et al., *An introduction to PYTHIA 8.2*, *Comput. Phys. Commun.* **191** (2015) 159 [arXiv:1410.3012] [INSPIRE].

[179] M. Drees et al., *CheckMATE: Confronting your Favourite New Physics Model with LHC Data*, *Comput. Phys. Commun.* **187** (2015) 227 [arXiv:1312.2591] [INSPIRE].

[180] D. Dercks et al., *CheckMATE 2: From the model to the limit*, *Comput. Phys. Commun.* **221** (2017) 383 [arXiv:1611.09856] [INSPIRE].

[181] J.S. Kim, D. Schmeier, J. Tattersall and K. Rolbiecki, *A framework to create customised LHC analyses within CheckMATE*, *Comput. Phys. Commun.* **196** (2015) 535 [arXiv:1503.01123] [INSPIRE].

[182] DELPHES 3 collaboration, *DELPHES 3, A modular framework for fast simulation of a generic collider experiment*, *JHEP* **02** (2014) 057 [arXiv:1307.6346] [INSPIRE].

[183] H. Jeffreys, *The Theory of Probability*, Oxford Classic Texts in the Physical Sciences (1939) [INSPIRE].

[184] L. Calibbi, J.M. Lindert, T. Ota and Y. Takanishi, *Cornering light Neutralino Dark Matter at the LHC*, *JHEP* **10** (2013) 132 [arXiv:1307.4119] [INSPIRE].

[185] G. Bélanger et al., *LHC constraints on light neutralino dark matter in the MSSM*, *Phys. Lett. B* **726** (2013) 773 [arXiv:1308.3735] [INSPIRE].

[186] K. Hamaguchi and K. Ishikawa, *Prospects for Higgs- and Z-resonant Neutralino Dark Matter*, *Phys. Rev. D* **93** (2016) 055009 [arXiv:1510.05378] [INSPIRE].

[187] J. Cao et al., *Testing the light dark matter scenario of the MSSM at the LHC*, *JHEP* **03** (2016) 207 [arXiv:1511.05386] [INSPIRE].

[188] R.K. Barman et al., *Invisible decay of the Higgs boson in the context of a thermal and nonthermal relic in MSSM*, *Phys. Rev. D* **95** (2017) 095018 [arXiv:1703.03838] [INSPIRE].

[189] R. Kumar Barman, G. Belanger and R.M. Godbole, *Status of low mass LSP in SUSY*, *Eur. Phys. J. ST* **229** (2020) 3159 [arXiv:2010.11674] [INSPIRE].

[190] W. Abdallah, A.K. Datta and S. Roy, *A relatively light, highly bino-like dark matter in the Z_3-symmetric NMSSM and recent LHC searches*, *JHEP* **04** (2021) 122 [arXiv:2012.04026] [INSPIRE].

[191] M. Van Beekveld, W. Beenakker, M. Schutten and J. De Wit, *Dark matter, fine-tuning and $(g-2)_\mu$ in the pMSSM*, *SciPost Phys.* **11** (2021) 049 [arXiv:2104.03245] [INSPIRE].

[192] R.K. Barman et al., *Is the light neutralino thermal dark matter in the MSSM ruled out?*, arXiv:2207.06238 [INSPIRE].

JHEP03(2023)198

[193] B. Fuks, M. Klasen, D.R. Lamprea and M. Rothering, *Gaugino production in proton-proton collisions at a center-of-mass energy of 8 TeV*, *JHEP* **10** (2012) 081 [arXiv:1207.2159] [INSPIRE].

[194] B. Fuks, M. Klasen, D.R. Lamprea and M. Rothering, *Precision predictions for electroweak superpartner production at hadron colliders with Resummino*, *Eur. Phys. J. C* **73** (2013) 2480 [arXiv:1304.0790] [INSPIRE].

[195] M. Chakraborti, S. Heinemeyer and I. Saha, *Improved $(g-2)_\mu$ Measurements and Supersymmetry: Implications for e^+e^- colliders*, in the proceedings of the *International Workshop on Future Linear Colliders*, (2021) [arXiv:2105.06408] [INSPIRE].

[196] ILC collaboration, *The International Linear Collider Technical Design Report — Volume 2: Physics*, arXiv:1306.6352 [ILC-REPORT-2013-040] [INSPIRE].

[197] CLIC Detector and Physics Study collaborations, *Physics at the CLIC e^+e^- Linear Collider — Input to the Snowmass process 2013*, in the proceedings of the *Community Summer Study 2013: Snowmass on the Mississippi*, (2013) [arXiv:1307.5288] [INSPIRE].

[198] CLICdp and CLIC collaborations, *The Compact Linear Collider (CLIC) — 2018 Summary Report*, arXiv:1812.06018 [CERN-2018-005-M] [DOI:10.23731/CYRM-2018-002] [INSPIRE].

[199] G. Alguero et al., *Constraining new physics with SModelS version 2*, *JHEP* **08** (2022) 068 [arXiv:2112.00769] [INSPIRE].

[200] PandaX-4T collaboration, *Dark Matter Search Results from the PandaX-4T Commissioning Run*, *Phys. Rev. Lett.* **127** (2021) 261802 [arXiv:2107.13438] [INSPIRE].

JHEP03(2023)198